UNIVERSIDADE DA BEIRA INTERIOR
Faculdade de Engenharia

Numerical Study of Freezing Droplets

Leandro Barbosa Magalhães

Dissertação para obtenção do Grau de Mestre em

Engenharia Aeronáutica

(ciclo de estudos integrado)

Orientador: Prof. Doutor André Rodrigues Resende da Silva

Covilhã, Maio de 2016

Acknowledgments

First and foremost I would like to take this opportunity to express my gratitude to my parents for their encouragement and support during my time at the University.

I would also like to thank my supervisor, Professor André Silva for his guidance throughout the development of this work, for his ability of solving apparent difficult questions with simple solutions and for his availability for every problem I had, which sometimes had nothing to do with this dissertation.

For last I wat to thank my colleague and friend Eduardo Antunes for his help with the idiosyncrasies of the FORTRAN computing language.

Resumo

O seguinte documento centra-se no estudo físico de processos de congelamento que se tornaram de extrema importância em engenharia aeronáutica. As causas mais comuns de danos estruturais em aeronaves devem-se a mudanças climatéricas como relâmpagos e o congelamento do bordo de ataque das asas ou das empenagens. O gelo espalha-se em direção ao bordo de fuga, afetando uma maior percentagem da superfície sustentadora em causa. Como resultado, surge uma necessidade de estudar e adaptar os modelos físicos e matemáticos existentes para uma melhor aproximação a situações reais, no sentido de uma diminuição da ocorrência de acidentes e incidentes resultantes deste tipo de fenómenos, contribuindo assim para melhores condições de aeronavegabilidade.
As previsões teóricas foram comparadas com dados experimentais e a análise numérica foi conduzida para a obtenção de uma melhor compreensão de processos de transmissão de calor e massa sob diferentes condições de humidade.

Palavras-chave

Transmissão de calor e massa, relações de Ranz-Marshall, razão de humidade

Resumo alargado

O documento seguinte dedica-se ao estudo físico de processos de congelamento que se tornaram de extrema importância em engenharia aeronáutica no sentido de garantir melhores condições de aeronavegabilidade.

As causas mais comuns de danos estruturais em aeronaves são originadas por fatores climatéricos com relâmpagos e ao congelamento de superfícies sustentadoras como asas ou empenagens. A formação de gelo numa destas superfícies (no bordo de ataque) expande-se em direção ao bordo de fuga, a temperaturas abaixo de 0ºC, afetando uma maior percentagem da superfície, diminuindo a sustentação. Existe assim uma necessidade de incorporar e adaptar os modelos existentes para uma maior aproximação a situações reais.

Uma revisão bibliográfica em que são abordados os princípios físicos de maior importância para este trabalho foi realizada tendo em conta várias aproximações matemáticas, com as suas vantagens e desvantagens e as condições segundo as quais se torna pertinente a sua aplicação num código de Dinâmica de Fluidos Computacional.

Numa segunda fase, modelos matemáticos representativos de várias situações que envolvem processos de congelamento são apresentados. Neste sentido, as previsões teóricas foram comparadas com dados experimentais para a validação do modelo numérico e para uma melhor compreensão dos processos físicos inerentes ao processo, como é o caso da transmissão de calor e massa sob diferentes condições de humidade.

Abstract

The present work is devoted to the numerical study of freezing processes which have become of major importance in aeronautical engineering. The most common causes of structural damage to aircrafts result from climacteric changes such as lightning strikes and icing of the wing's leading edges or empennage, which turns the smooth airflow over the wings into turbulent. At subzero temperatures, icing spreads from the leading to the trailing edge, affecting a greater percentage of the wings.

As a result there is a need to study and adapt existing physical and mathematical models to achieve a better approximation to real life situations in order to mitigate the occurrence of incidents and accidents involving aircraft for a better continuous airworthiness.

The theoretical predictions are compared against experimental data and the numerical analysis is conducted to provide insight into heat and mass transfer processes under several humidity conditions.

Keywords

Heat and mass transfer, Ranz-Marshall relations, humidity ratio

Table of Contents

List of figures

List of tables

Nomenclature

A	droplet surface area
B	model constant
C	model constant
C_D	drag coefficient
c_L	specific heat conductivity of liquid
c_S	specific heat conductivity of solid
C_{pd}	drop specific thermal capacity
C_p	water specific heat
$C_{p\gamma}$	semi solid drop heat capacity
C_{pl}	liquid drop heat capacity
C_{ps}	solid drop heat capacity
d	drop diameter
dh_f	water enthalpy variation
dW	humidity variation within the control volume
E	emissivity
D	mass diffusivity
D_{vg}	gas or vapor thermal diffusivity
G	correction factor
h_c	convective heat transfer coefficient
h_d	convective mass transfer coefficient
h_{fg}	water vaporization enthalpy
K_d	heat conduction inside the drop
K_L	thermal conductivity in liquid
k_S	thermal conductivity in solid
L	latent heat
Le	Lewis number
L_f	latent heat due to crystallization
m_a	air mass flow
m_w	water mass flow
Nu	Nusselt number
P_L	Navier-Stokes tensor
Pr	Prandtl number
q_L	conductive heat flow
q_h	convective heat flow
q_m	mass heat flux
q_r	thermal radiation

Re	Reynolds number
Sc	Schmidt number
S_d	drop area
Sh	Sherwood number
St	Stefan number
T_d	drop temperature
T_g	ambient temperature
T_m	melt temperature/ phase change temperature
T_n	nucleation temperature (empiric value)
T_s	Temperature of the drop completely solidified
U	drop velocity
$\vec{v}$	velocity field
V_d	drop volume
V_r	drop-gas relative speed
W_s	Saturation humidity rate
W_∞	environment humidity rate

Greek symbols

ρ_L	liquid density
ρ_S	solid density
N	kinematic viscosity
μ	dynamic viscosity
τ	time
σ	Stefan-Boltzmann constant
α	thermal diffusivity
θ	model constant
ε	total energy
ξ	Similarity variable

Acronyms

SIS	Smart Icing Systems
IPS	Ice Protection System
IMS	Ice Management System
NASA	North American Space Agency
PCM	Phase Change Material
PDE	Partial Differential Equation

FDE	Finite difference Equation
CFL	Courant-Friedrichs-Lewy
SOR	Successive Over Relaxation

1. Introduction

1.1. Introduction

The present work is devoted to the numerical study of freezing processes which have become of major importance in aeronautical engineering. According to Caliskan and Hajiyev (2013), the most common causes of structural damage to aircrafts due to climacteric changes are the result of lightning strikes and icing at the wing's leading edge or empennage.
The icing of a wing's leading edge turns the smooth airflow over the wing into a turbulent one, decreasing lift and increasing drag as seen in figure 1.1. At temperatures below zero, icing spreads to the trailing edge, affecting more of the wing.

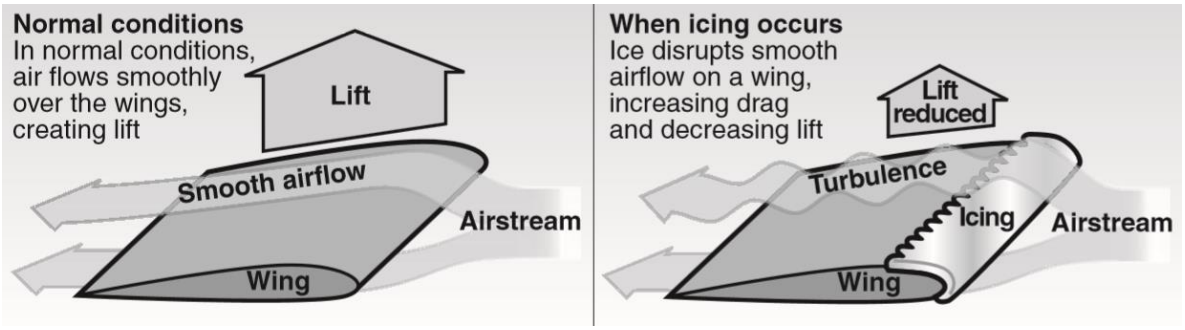

Figure 1.1. Effect of icing on an aircraft wing, Dillingham 2010

Overall, icing has a negative effect on the aircraft's aerodynamic performance, especially during take-off and landing and anti-icing systems on modern aircrafts make use of the heat exhausted from the engines, to prevent the ice from forming, which increases fuel consumption and in turn the operational costs of the aircraft. As a result, SIS (Smart Icing Systems) have been the focus of many studies.
SIS measure the ice accretion with the aircraft performance degradation and then the information is transmitted, in order to control the Ice Protection System (IPS) and if necessary to adjust the flight controls to the situation, coordinated with the flight crew.
Ice accretion can be divided into several categories, depending on the phenomenon responsible for them – the initial ice accretions on the lifting surfaces before or after anti-icing systems are deployed, which can be underestimated or neglected; runback or ridge ice accretions after the IPS is deployed, for the fact it reduces the aerodynamic effectiveness of the control surfaces; shaped ice accretions in aircraft without IPS or system failure. A detailed explanation of the various types of ice accretion is described in Cao and Wu (2014).

The icing on aircrafts can be approached in three different ways: flight test, of the three the most reliable and accurate, wind tunnel experiment with artificially simulated ice shape and numerical simulation; icing is basically a fluid structure interaction process. For numerical calculation, it is considered a quasi-steady process.

Another negative effect of ice on aviation relates to the impact of hail particles, which can contribute to serious damage on aircraft structures and jet engines – power loss and flameouts. Many studies were conducted on this subject – Hauk *et al* 2015 formulated and validated models for the impact of ice crystals onto solid walls and were able to document the velocity where no fragmentation occurs.

Overall the formulation and integration of a suitable model for icing protection on an aircraft is composed of two parts. An adequate numerical model which fully describes the aerodynamic performance degradation to be used by a flight control model, to create an Ice Management System (IMS). The main purposes of the IMS consists on the detection of the existence of ice accretion and its effects on flight dynamics and the activation and management of the IPS and ensuring the pilot with the description of the icing effects.

The need for further studies on aircraft's icing remains of critical importance given the amount of incidents on record, which given the unpredictability on the conditions icing is encountered could contribute to increase fatalities and material losses. These records were collected by Dillingham (2010) from the NASA (North American Space Agency) database and divided into several categories, according to the effect icing had on aircraft operation and are here presented in table 1.1.

Table 1. 1. Icing and Winter Weather-Related Incident Reports for Large Commercial Airplanes by Category of Incident, 1998 to 2007, Dillingham 2010

Category	**Number of Reports**
Anti-ice or deicing incident/procedure	179
Controllability issue-ground	72
In-flight encounter-aircraft equipment problems	72
In-flight encounter-airframe and/or flight control icing	69
Other winter weather incident	42
Surface marking and signage obstruction	41
Runway, ramp, or taxiway excursion	36
Runway, ramp, Or taxiway incursion	34
Controllability issue-air	32
Maintenance incident	19
Ramp safety-personnel risk or injury	17
In-flight encounter-sensor type incident	15
Total	**628**

In a concluding remark, the present work has the objective of becoming a stepping stone for further studies in the development of a model capable of simulating ice accretion and the impact of ice crystals into solid surfaces, incorporating previous works as it will be the case of the evaporation model.

1.2. Overview

The present thesis is organized in 5 chapters. The current – chapter 1 – presents the work's scope; the impact icing phenomena has on aircraft operations and its consequences, all supported by historical data, in order to try to understand the present and attempt to predict the future. In chapter 2 a bibliographic review is presented of the most relevant research of the subject at hand up to now, including mathematical and physical concepts considered fundamental in the development and understanding of this study.

Chapter 3 relates to the modelling of cooling and freezing of fluids under several conditions. Here the model for the freezing of a system of water drops in free fall is presented and later on the cooling stage is incorporated into a four phase freezing model, already including supercooling, recalescence and nucleation stages.

In chapter 4 an analysis of the results is undertaken and the influence of the different parameters studied with their practical implications is taken into account.

For last, the final chapter – chapter 5 – presents the main findings and conclusions of this work as well as suggestions of how this research can be continued in the future.

2. Bibliographic review

2.1. Introduction

In 1952 Ranz and Marshall have conducted an experimental study focused on drops' evaporating rates. The most important conclusion of this study resulted in the confirmation of the analogy between heat and mass transfer. They have also presented correlations for the Nusselt and Sherwood's numbers in terms of the Reynolds, Schmidt and Prandtl ones.

Also in 1952, Hughes and Gilliland studied the behavior of drops and sprays under a dynamics point of view.

Around the sixties the interest in ice led to studies focused on the relation between supercooled drops of water and its radius and supercooling degree. In 1961, Glicki and Mardonko showed that drops with a diameter less than 300 μm can solidify into a single crystal, being more common with low levels of supercooling. The mechanism responsible for the freezing, however was not mentioned.

In 1968, Dickinson and Marshall considered the mean drop diameter, size distribution and initial velocities and temperatures in their studies.

Yao and Schrock, in 1976, conducted experiments about heat and mass transfer in free falling drops above 0 up to the range of the terminal velocity. They also modified the Ranz-Marshall expressions to include the effects of acceleration.

At the beginning of the 80's, Zarling focused his studies on a theoretical and numerical analysis of a system of drops in free fall, in order to evaluate variations in the humidity ratio, enthalpy and the drop's own temperature.

In 1993, Alexiades and Solomon made a summarized the evolution of models from the most basic Stefan problem to hints and clues to program the numerical models on FORTRAN.

More recently in 1997, Griebel *et a*l developed a model based on the SIMPLE scheme, with the help of the Navier-Stokes equations and the Gibbs-Thomson effect, to account for density variations across the interface on a phase change process.

An application of heat and mass transfer theories applied to freely falling drops at low temperatures was used as a way to separate clean water from industrial waste. Gao *et al* (2000) made such a study based on the fact when drops freeze, the crystal growth results only of pure water, leaving the waste particles in an unfrozen liquid state.

Hindmarsh *et al* (2003) and Tanner (2011), worked on a four stage freezing model (supercooling, nucleation, recalescence and crystallization), with the incorporation of thermocouples, and later a more detailed three stage model (without supercooling). Their model was validated for a single cocoa butter and spray.

2.2. Physical phenomena

In order to fully understand how the phase change of a material occurs, it is necessary to discuss some relevant physical phenomena and mathematical concepts.

Both phases are characterized by the presence of cohesive forces which keep the atoms in close proximity to each other and their movement is related to equilibrium positions. While in liquids the atoms jump between these positions, in solids they vibrate around them. The macroscopic manifestation of this vibrational energy is called heat or thermal energy, the measure of which is the temperature. As a result, it is possible to conclude that atoms in the liquid phase are more energetic (hotter) than those in the solid one.

Before a solid can melt, it is necessary for him to acquire a certain amount of energy, in order to break the cohesive forces that hold its solid structure. This energy is called latent heat and represents the difference in thermal energy between the solid and liquid state. On the other hand, the freezing of a liquid requires the removal of latent heat. In either cases there is a rearrangement of the material's entropy, which is a characteristic of first order phase transitions. In a first order transition, solidification happens through a crystallization process where both the solid and the liquid phases coexist. This is opposed to a second order transition, where solidification occurs as the temperature is continuously increased.

In a more direct approach, the transition from one phase to another, meaning the absorption or release of latent heat occurs at a temperature at which the stability of one phase breaks in favor of the other, accordingly to the available energy. The phase change temperature or melt temperature depends on the pressure. It is of high importance to state the thermophysical properties that vary linearly with the temperature may suffer a nonlinear variation at the phase change temperature. The process of phase transition from solid to liquid and liquid to solid is fully described in Alexiades and Solomon (1993), in theoretical terms.

Another relevant feature is the molecular structure: the formation of any crystal requires the movement of atoms to the forming crystalline structure, and so it may happen the temperature of the material be cooled down below the melt temperature, without the formation of a solid. A liquid in this situation is referred to in literature as supercooled (the difference between a normal cooling and a supercooling is well visible in figure 2.1). There can also be the case in which a liquid is cooled to an extremely low temperature that the latent heat is not enough to raise its temperature to the phase change. In this case the liquid is labeled hypercooled. The subsequent solidification of a supercooled liquid is called flash freezing. On the other hand, a material can also be cooled below T_m and remain in its liquid phase – undercooled melt. If the liquid is cooled even further, it will eventually reach nucleation and solidification begins, after which recalescence takes place. A report by Robinson (1981) presents several theoretical hypotheses trying to give an answer to the question of how much a material can be undercooled before nucleation occurs.

The supercooling level will leave its mark at the drop's final microstructure. As higher the supercooling level is, the biggest will the drop's portion with a crystalline structure be (Hindmarsh *et al* 2007).

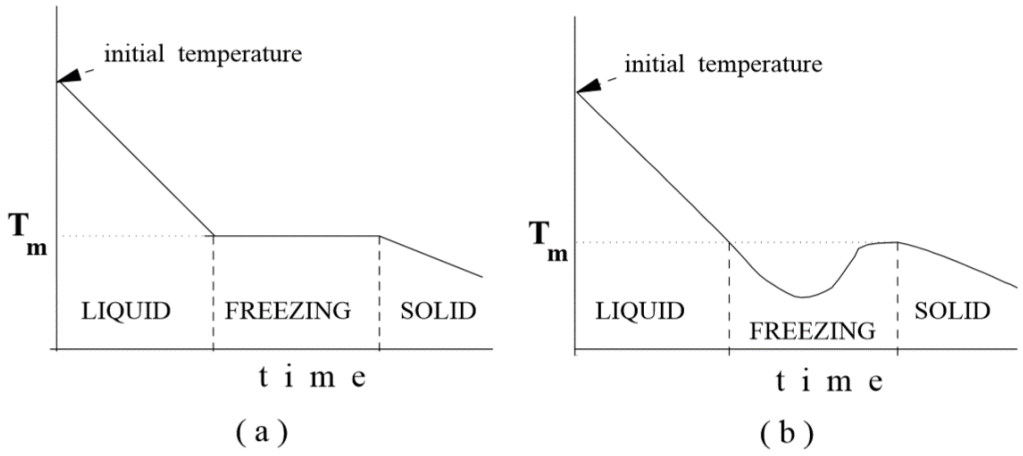

Figure 2.1. Normal cooling (a) vs supercooling (b), Alexiades et al 1993

The melt temperature, as established before is the temperature at which both solid and liquid phases coexist. At a given temperature higher than the melt temperature, the free energy of the liquid is less than that of the solid, so accordingly to thermodynamics second law, the liquid phase is the stable one.

The supercooled state is metastable and $\Delta T = T_m - T$ is the supercooling degree. A metastable state means the free energy is higher than that of the real stable state – the solid. Therefore, this is a local state of minimal energy and not global. There's a barrier that keeps the system from reaching its stable state, due to nucleation problems.

Nucleation is the process, where the molecules start to rearrange themselves in clusters, forming small crystals within the liquid.

The phase change region where both phases coexist is called interface. The interface's structure can be influenced by the material itself, the cooling rate, the liquid phase temperature gradient and surface tensions. As a consequence the interface's structure can be planar, dendritic or amorphous. If the interface is a curve with a mean curvature of de $\frac{1}{2}k$, the local freezing temperature is given by the Gibbs-Thomson relation. As fundamental as it can be for the interface, the Gibbs-Thomson effect is usually insignificant to the global heat transfer process.

2.3. The Stefan problem

The Stefan problem is a simple mathematical model for the characterization of phase change processes, which initially incorporates only the most basic phenomenon – Classical Stefan

Problem. From this model, it is possible do develop increasingly complex ones, through the addition of effects that were initially left out. The most common considerations and assumptions done in this type of problems are presented in table 2.1.
The objective of the Stefan problem will be to discover the two unknown common to all phase change problems: the temperature field and the location of the interface. Such a model has been used in areas like molecular diffusion, friction and lubrication, combustion, inviscid flow, slow viscid flow and flow in porous surfaces. Although the moving interface's location is calculated through a sequence of conditions and equations, the amount of calculation done to advance one time step can be reduced to that of a problem with a fixed boundary (Shampine *et al*).

Let us now consider a two phase Stefan problem as presented by Alexiades and Solomon (1993):

> **Physical problem:** *Melting of a semi-infinite slab, $0 \leq x \leq \infty$, initially solid at a uniform temperature $T_s \leq T_m$, by imposing a constant temperature $T_L > T_m$ on the face $x=0$. Thermophysical parameters ρ, c_L, c_s, k_L, k_S, L, $\alpha_s = \frac{k_S}{\rho c_s}$, $\alpha_L = \frac{k_L}{\rho c_L}$, all constant. The schematic representation of this problem can be observed in* figure 1.2.

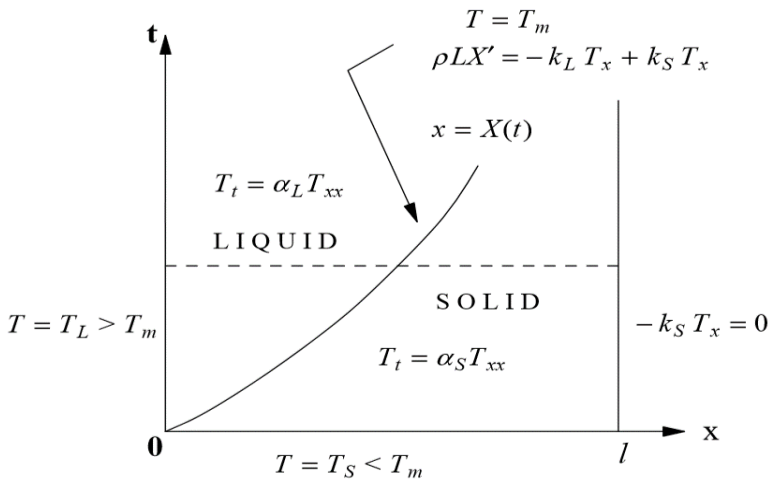

Figure 2.2. Two phase Stefan problem, Alexiades et al 1993

Physically, the above problem represents a tube filled with a PCM - Phase Change Material, being one of the phases exposed to a heat source, while the length of the tube is so high that the melting front cannot reach the other phase during the experiment.

Table 2.1. Overview of the most common assumptions on the Stefan problem, Alexiades et al 1993

Physical factors involved in phase change processes	**Simplifying assumptions for the Stefan problem.**	**Remarks on the assumptions**
1.Heat and mass transfer by conduction, convection, radiation with possible gravitational, elastic, chemical, and electromagnetic effects	Heat transfer isotropically by conduction only, all other effects assumed negligible.	Most common case. Very reasonable for pure materials, small container, moderate temperature gradients.
2.Release and absorption of latent heat	Latent heat is constant; it is released or absorbed at the phase-change temperature.	Very reasonable and consistent with the rest of the assumptions.
3.Variation of phase-change temperature	Phase-change temperature is a fixed known temperature, a property of the material.	Most common case, consistent with other assumptions.
4.Nucleation difficulties, supercooling effects	Assume not present.	Reasonable in many situations.
5.Interface thickness and structure	Assume locally planar and sharp (a surface separating the phases) at the phase change temperature.	Reasonable for many pure materials (no internal heating present).
6.Surface tension and curvature effects at the interface	Assume insignificant.	Reasonable and consistent with other assumptions.
7.Variation of thermophysical properties	Assume constant in each phase, for simplicity ($c_L \neq c_S$, $k_L \neq k_S$).	An assumption of convenience only. Reasonable for most materials under moderate temperature variations. The significant aspect is their discontinuity across the interface, which is allowed.
8.Density changes	Assume constant ($\rho_L = \rho_S$).	Necessary assumption to avoid movement of the material. Possibly the most unreasonable of the assumptions.

As said before the objective is to discover the temperature distribution T(x,t) as well as the interface location X(t), accordingly to the following conditions:
Heat equation in the melting region:

$$T_t = \alpha_L T_{xx}, \quad 0 < x < X(t), \quad t > 0 \tag{2.1a}$$

Heat equation in the solid region

$$T_t = \alpha_s T_{xx}, \ X(t) < x, \ t > 0 \tag{2.1b}$$

Interface temperature

$$T(X(t), t) = T_m, \quad t > 0 \tag{2.1c}$$

Stefan's condition

$$\rho L X'(t) = -k_L T_x(X(t)^-, t) + k_S T_x(X(t)^+, t), \ t > 0 \tag{2.1d}$$

There is a convention where the solid corresponds to the negative sign, while the liquid is given by the positive one.
The right hand side of equation 2.1d represents a change in the heat flux q_L-q_S in x=X(t). The notation $T_x(X(t)^{\pm}, t)$ is used to remember these values are the limit of $T_x(x,t)$, when $x \to X(t)^{\pm}$.

Initial conditions

$$T(x,0) = T_S < T_m \,, x > 0, \ X(0) = 0 \tag{2.1e}$$

Boundary conditions

$$T(0,t) = T_L > T_m, \quad \lim_{x\to\infty} T(x,t) = T_S \,, \quad t > 0 \tag{2.1f}$$

2.3.1. The Neumann solution

In this section will be discussed a method for the solvability of the Stefan problem. Let us begin with the introduction of the similarity variable:

$$\xi = \frac{x}{\sqrt{t}} \tag{2.2}$$

Therefore, we are seeking a solution in the form of:

$$T(x,t) = F(\xi) \tag{2.3}$$

The function $F(\xi)$ is unknown. On the other hand, the location of the interface is proportional to $\sqrt{t}$. As a result there is a proportional constant A which must be found.

$$X(t) = A\sqrt{t} \tag{2.4}$$

Now, replacing in equation 2.1 and integrating, it is possible to obtain the new equation 2.5, with B and C as constants.

$$F(\xi) = B\int_0^{\xi} e^{\frac{s^2}{4\alpha_L}}\,ds + C = B\sqrt{\pi\alpha_L}\,\mathrm{erf}\left(\frac{\xi}{2\sqrt{\alpha_L}}\right) + C \tag{2.5}$$

At this point, it is of good practice to reformulate the initial problem, to accommodate the similarity solution. As such the objective is to discover the solution of $X(t) = 2\lambda\sqrt{\alpha_L t}$, for $T(x,t) = F_L(\xi)$, in the liquid phase and for $T(x,t) = F_S(\xi)$ in the solid one, being λ an unknown constant and F_L and F_S unknown functions of the similarity variable (ξ). Then the new formulation is given by:

Interface location

$$X(t) = 2\lambda\sqrt{\alpha_L t},\quad t > 0 \tag{2.6a}$$

Temperature in the liquid phase $0 < x < X(t),\quad t > 0$

$$T(x,t) = T_L - (T_L - T_m)\frac{\mathrm{erf}\left(\frac{x}{2\sqrt{t\alpha_L}}\right)}{\mathrm{erf}(\lambda)} \tag{2.6b}$$

Temperature in the solid phase $x > X(t),\quad t > 0$

$$T(x,t) = T_S + (T_m - T_s)\frac{\mathrm{erf}\left(\frac{x}{2\sqrt{t\alpha_S}}\right)}{\mathrm{erf}\left(\lambda\sqrt{\frac{\alpha_L}{\alpha_S}}\right)} \tag{2.6c}$$

Solution of the transcendental equation (λ)

$$\frac{St_L}{\exp(\lambda^2)\mathrm{erf}(\lambda)} - \frac{St_S}{\nu\exp(\nu^2\lambda^2)erfc(\nu\lambda)} = \lambda\sqrt{\pi} \tag{2.6d}$$

with:

$$St_L = \frac{c_L(T_L - T_m)}{L},\ St_S = \frac{c_L(T_m - T_S)}{L},\ \nu = \sqrt{\frac{\alpha_L}{\alpha_S}} \tag{2.7}$$

The factors St_L and St_S present in equation 2.7 represent the Stefan number for a melting and freezing process, which notes the quotient between sensible and latent heat. The sensible heat is described as the one that is related to the temperature increasing. Therefore:

$$sensible\ heat = \int_{T_m}^{T} C(T)dT \tag{2.8}$$

The objective of the Stefan number is to determine if a given method is appropriate to analyze the phase change process. While high Stefan numbers mean the process will be of pure conduction, low magnitude numbers state it will be dominated by the phase change.

Another notable aspect is related with the enthalpy. At $T=T_m$, the enthalpy has a jump of magnitude L. Any region in which $T=T_m$ and $0<e<L$ is referred as a mushy zone. Accordingly to the number 5 of table 2.1 the interface's thickness will be equal to 0.

The transcendental equation has only one solution for $\lambda > 0$, which means the similarity solution is unique for $St_L > 0$, $St_S \geq 0$, , $\nu > 0$.

For a two phase freezing process, the Neumann solution is obtained changing the subscripts L for S and the latent heat from L to –L.

The interface is the frontier that divides the solid and liquid regions, meaning there is a need for a frontier condition for each phase in order to achieve a solution. It is given the temperature must be continuous and at T_m follows an isotherm, translated into:

$$\lim_{\substack{\vec{x}\to interface \\ \vec{x}\in liquid}} T(\vec{x},t) = T_m \tag{2.9}$$

$$\lim_{\substack{\vec{x}\to interface \\ \vec{x}\in solid}} T(\vec{x},t) = T_m \tag{2.10}$$

If the interface location was known, there would be a necessary conditions to determine the temperature in each phase.

Regarding the Stefan condition, introduced in this subsection, it denotes the latent heat released due to movement of the interface equals the flux of heat per unit time. As a result, the Stefan condition represents a heat balance across the interface.

In other words, the Stefan condition shows the latent heat rate change $\rho L X'(t)$ equals the heat that jumps across the interface. In particular, the heat flux can be continuous if and only if L=0 or the interface does not move. When discussing a cylinder or a sphere the characteristic length is the radius.

In a final note, the functions T(x,t) and X(t) constitute a solution to the Stefan problem up to a time t*, if the functions' derivatives of every order, which appear in the problem formulation are continuous and satisfy the problem conditions. The time t* designates the time up to which the solution is desired.

There are methods called front tracking schemes, which try to find the interface's location through the Stefan number.

2.4. Density considerations

Changes in density induce movement of the material and further complicate the modeling of phase change processes. For most materials $\rho_L<\rho_S$, meaning they expand upon melting, which creates containment issues.

There are two different kinds of density change of particular importance in phase change processes. The first one is the already mentioned difference between phases, the other being the density variation with temperature. A liquid density diminishes with the increasing temperature and as a consequence, much hotter the liquid is, more volume will occupy. In the presence of gravity, a temperature gradient induces a flux due to buoyancy called natural convection, modeled by the Rayleigh number.

Let us consider the case of a shrinking in a closed container with $\rho_L<\rho_S$. The formatting solid occupies less volume as a consequence of the relation between densities. Therefore the container gets under pressurized. From this point, two consequences were theorized: either the container or the PCM will break. If the container is strong enough, voids are formed, fulfilled with the material's vapor. The place where they form depends on the magnitude of the adhesion forces: wall-liquid, wall-solid, liquid-solid or within the liquid or the solid. Usually the weakest forces are registered between the wall and the PCM.

There is also the possibility of microbubbles of pre-existent air be trapped within the liquid. These bubbles will fluctuate to the top- buoyancy- even in zero gravity- Marangoni flow- due to the surface tensions. Marangoni result from either temperature of chemical concentration gradients at the interface.

The modulation of these complicated phenomenon is approached in the context of energy storage in space systems, with resource to the Navier-Stokes equations and thermodynamic knowledge of the interface.

2.5. Approximations

The most important characteristic of the explicit solutions in phase change problems is that they provide real insight of how the different parameters at study interact with the factors of interest to us.

The number of problems with explicit solution is extremely low and in most cases, they don't have relevance in real life situations. Explicit solutions exist to problems with constant parameters in each phase and imposed temperature, which leaves imposed flux out of the picture.

As a result, there is a need to use approximations: analytical and numerical. The downside arises from the fact that there is no way of verify the validity of the simplifications and there are no error approximations to the mathematical ones. On the other hand, there are problems that remain even when a system is reduced to its most basic form. Examples can be found in Temos *et al* (1996), regarding mass transfer. There, they pay a closer look to mass transfer in initially insulated droplets and conclude that even for such a system there are several problems as:

I. Interface contamination, which will reduce the mass transfer, when compared with a pure system;
II. Interface instability, with the consequence of pressure gradients that will increase the mass flow (Marangoni)
III. Hydrodynamic changes within the droplet, due to stagnation in oscillation, which influences the boundary layer and vortex shedding.

It has become clear by previous studies, the mass transfer is deeply affected by hydrodynamic factors. However a detailed explanation of the droplet dynamics is only available for special cases, but generalizations can be built with the drag coefficient graphic as seen in Temos *et al* (1996).

2.5.1. Analytical approximations

The validity of an analytical approximation is made from comparison with the results of other independently validated method. These provide qualitative and magnitude information, instead of just quantitative.
Now the main analytical approximations will be introduced, as well as their most relevant aspects.

2.5.1.1. Quasistationary approximation (Alexiades *et al* 1993)

I. Simplify the heat equation to its steady state
II. One phase method (Cartesian, cylindrical or spherical coordinates)
III. The sensible heat is negligible in comparison to the latent heat (Stefan number)
IV. Overestimate the interface location
V. Simple for determination of the feasibility and estimate sizing of the problem
VI. First cut answers, which through any other way would require costly computational estimation.
VII. Low accuracy

2.5.1.2. Megerlin method (Alexiades *et al* 1993)

I. Assume parabolic temperature profile
II. May be difficult to use
III. If the boundary data are not constant, there won't be an explicit solution
IV. Solvability with convective boundary conditions
V. It can violate the conservation of energy, since this equation is only satisfied at the boundary

2.5.1.3. Heat balance integral method (Sethian *et al* 1993 & Lunardini 1981)

I. Assume parabolic temperature profile
II. May be difficult to use
III. Seeks to satisfy a global heat balance explicitly
IV. Given the impossibility of error determination, the choice between this method and the Megerlin method becomes a matter of personal preference

2.5.1.4. Perturbation method (Alexiades *et al* 1993)

I. Uses mathematical expansion in series to reduce a larger problem into simple ones with explicit solution
II. Represents a high order correction of the quasistacionary approximation
III. Convenient and efficient dimensionless formulation
IV. Interface location is fixed in space

2.5.2. Numerical approximations (Caginalp *et al* 1991 and Fix *et al* 1988*)*

There are several aspects of numerical approximations common to all algorithms that are presented next:

I. Physical region approximated by a small number of control volumes
II. Idealized mathematical concepts like integrals and derivatives must be re-approximated by finite-differences methods
III. The most common numerical method for the simulation of phase change processes
IV. High temperature gradients require the use of small control volumes and small temperature gradients can be acquired by large control volumes
V. Control volumes are regions where local equilibrium is achieved in a time scale smaller than the time step
VI. Finite-differences result from control volume discretization

The numerical approximations may be divided into different paths, depending on the objectives of the work. Let us then define the mathematical work region.
The region M is divided into control volumes. To each sub region V_j is associated a node x_j. There is also a need to define ΔV_j as the volume of V_j and $A_{ij}=A_{ji}$ the common area of V_i e V_j.
As a result, the two main schemes are:

Explicit scheme:

$$E_j^{n+1} = E_j^n + \frac{\Delta t_n}{\Delta x_j}\left(q_{j-1/2}^n - q_{j+1/2}^n\right), j = 1, \dots, M, \;\; n = 0,1, \dots \tag{2.11}$$

Fully implicit scheme:

$$E_j^{n+1} = E_j^n + \frac{\Delta t_n}{\Delta x_j}\left(q_{j-1/2}^{n+1} - q_{j+1/2}^{n+1}\right), j = 1, \dots, M, \;\; n = 0,1, \dots \tag{2.12}$$

The quotient between length and thermal conductivity is defined as thermal resistance, where the temperature drop ΔT is called thermal driving force:

$$thermal\ resistence = \frac{length\ of\ resistance\ path}{(crossectinal\ area)*(conductivity)} \tag{2.13}$$

The standard centered difference discretization of T_{xx} is given by equation 2.14. For plain heat conduction, as defined when we discussed the Stefan problem, the total energy is the sensible heat. Also, due to irregularities at the interface, the thermal conductivity is not a constant, but a function of the position.

$$E_j^{n+1} = E_j^n + \frac{k\Delta t_n}{\Delta x^2} * (T_{j-1}^{n+\theta} - 2T_j^{n+\theta} + T_{j+1}^{n+\theta}) \tag{2.14}$$

The discrete problem is then defined as:

Initial values: $T_j^0 = T_{init}(x_j), j = 1, \dots, M$ (2.15a)

Boundary condition at x=0: $q_{1/2}^{n+\theta} = -\frac{T_1^{n+\theta} - T_\infty^{n+\theta}}{\frac{1}{h} + R_{\frac{1}{2}}}, \quad R_{1/2} = \frac{1/2\Delta x}{k_1}$ (2.15b)

Boundary condition at x=l: $q_{M+1/2}^{n+\theta} = 0$ (2.15c)

Interior values: $T_j^{n+1} = T_j^n + \frac{\Delta t_n}{\rho c_j \Delta x_j} * \left(q_{j-1/2}^{n+\theta} - q_{j+1/2}^{n+\theta}\right), j = 1, \dots, M$ (2.15d)

Where: $q_{j-1/2}^{n+\theta} = -\frac{T_j^{n+\theta} - T_{j-1}^{n+\theta}}{R_{j-1/2}}$, with $R_{j-1/2} = \frac{1/2\Delta x_{j-1}}{k_{j-1}} + \frac{1/2\Delta x_j}{k_j}, j = 2, \dots, M$

and

$$T^{n+\theta} = (1-\theta)T^n + \theta T^{n+1} \tag{2.15e}$$

In this case, the discretization replaces a partial differential equation ($PDE[u] = 0$) by a finite-difference equation ($FDE\left[u_j^n\right] = 0$). A consistent finite-difference method for a well posed problem is convergent if and only if is stable – Lax equivalence theorem.

The local truncation error is given by:

$$te_j^n \coloneqq FDE[u(x_j, t_m)] \tag{2.16}$$

The local discretization error is given by:

$$de_j^n \coloneqq U_j^n - u(x_j, t_n) \tag{2.17}$$

The simplicity and convenience of the explicit scheme is posed against the restraint necessity of the time step, in order to achieve numerical stability of the formulation.

The stability condition known as CFL-Courant-Friedrichs-Lewy is:

$$\Delta t \leq \frac{1}{2}\frac{\Delta x^2}{\alpha} \tag{2.18}$$

Errors are represented by Fourier series expansions and typical Fourier amplification factors are calculated.

A simple method to achieve stability is the "*positive coefficient rule*" fully described in Patankar *et al* 1980 and Anderson 1995, where T_j^{n+1} is written as a linear combination of its neighbors.

The CFL condition can be altered when facing different boundary conditions:

$$\Delta T_n < \frac{1}{3}\frac{\Delta x_{min}^2}{\alpha_{max}} \tag{2.19}$$ for imposed temperatures and convective conditions

$$\Delta T_n < \frac{1}{2}\frac{\Delta x_{min}^2}{\alpha_{max}} \tag{2.20}$$ for imposed flux conditions

There is a recommendation in the literature to use the fully implicit discretization to boundary nodes.

2.5.2.1. Enthalpy formulation (Smith 1981)

The main features of this formulation are presented below:

I. Bypasses the explicit track of the interface. The Stefan condition is met automatically as a natural boundary condition
II. The enthalpy formulation (also referred to in literature as weak formulation) is very similar to the method used in gas dynamics to chocking.
III. The enthalpy method discretized by finite differences is the most versatile, convenient and the simplest to program in phase change problems in 1,2 and 3D. (However it does not solve every problem)
IV. The volume occupied with the PCM is divided in an infinite number of control volumes V_j and then, energy conservation is applied, meaning a discrete energy balance is used to update the enthalpy at every control volume
V. The phases are determined just by the enthalpy, with no mention to the interface location - volume tracking scheme (Sullivan *et al* 1987)

The discrete problem is defined as:

Initial values: $T_j^0 = T_{init}(x_j), \quad j = 1, \dots, M$ (2.21a)

Boundary condition at x=0: $q_{1/2}^{n+\theta} = -\frac{T_1^{n+\theta} - T_\infty^{n+\theta}}{\frac{1}{h} + R_{\frac{1}{2}}}, \quad R_{1/2} = \frac{1/2\Delta x}{k_1}$ (2.21b)

Boundary condition at x=1: $q_{M+1/2}^{n+\theta} = 0$ (2.21c)

Interior values: $E_j^{n+1} = E_j^n + \frac{\Delta t_n}{\Delta t_j}\left[q_{j-\frac{1}{2}}^{n+\theta} - q_{j+\frac{1}{2}}^{n+\theta}\right], \ j = 1, \dots, M$ (2.21d)

With:

$q_{j-1/2}^{n+\theta} = -\frac{T_j^{n+\theta} - T_{j-1}^{n+\theta}}{R_{j-1/2}}$, com $R_{j-1/2} = \frac{1/2\Delta x_{j-1}}{k_{j-1}} + \frac{1/2x_j}{k_j}, j = 2, \dots, M$ (2.21e)

And

$$f(x) = \begin{cases} T_m + \frac{E_j^n}{\rho c_S}, \ E_j^n \leq 0 \quad (solid) \\ T_m, \ \ 0 < E_j^n \leq \rho L \ \ (interface) \\ T_m + \frac{E_j^n - \rho L}{\rho c_L}, E_j^n \geq \rho L \quad (liquid) \end{cases} \quad (2.22)$$

The algorithm presented previously has the following methodology: knowing the temperature and the phase of each control volume, the resistances are computed and the fluxes, which are then used to update the enthalpies that produce new temperatures and phase states.
In situations where the time step must be small for physical reasons, the explicit scheme may turn out to be as efficient as the implicit one.
The implicit scheme is more advantageous for slow phase change processes than for faster ones.
Explicit schemes have inherent limitations in relation to the time step, imposed by the stability conditions. On the other hand, even fully implicit schemes must have restrictions regarding the time step, to attain precision. The loss of precision occurs when the following is not respected:

$$|X'|\Delta t \leq \Delta x \tag{2.23}$$

The faster the melting process is, the lower will the time step be, in order to have acceptable precision. Therefore the implicit scheme is less advantageous. The explicit scheme is mainly used to exploratory studies.
The enthalpy method is flexible enough to allow the sample (wall + PCM) to be treated as a unique region, but with different thermophysical properties to both phases.
The basic limitation of the classical formulation, as seen before, lies with the fact the interface must be assumed a sharp interface. This is particularly problematic when discussing cyclic melting/freezing problems, where several interfaces are likely to appear. In this case, it would be necessary to know the interfaces structures a priori.
Even with numerical approximations there are problems in which the mathematical models are not totally adequate like biphasic flows. As a result, there is the need to use experimental data to validate the model. On the other hand it is necessary to develop the models so they approximate more the physical processes.

3. Mathematical models

3.1. Introduction

In this chapter first a mathematical model for the calculation of heat and mass transfer on a system of free falling drops is described. Then a four phase freezing model with supercooling is introduced. This chapter concludes by describing the initial conditions to be used in the numerical simulations, as well as the computational domain configuration.

3.2. Heat and mass transfer on a system of free falling drops

This section describes a model for the calculation of heat and mass transfer coefficients for a system of free falling drops in moist air conditions. It starts by presenting and explaining the processes behind a single drop modulation and then it evolves until the procedure for the calculations of a system of drops is presented.

According to Hindmarsh *et al* (2003), the techniques used for the analysis of water droplets can be divided into two categories: free flight, which is the current case and levitation. Levitation is further divided into intrusive and non-intrusive techniques, exemplified in figure 3.1.

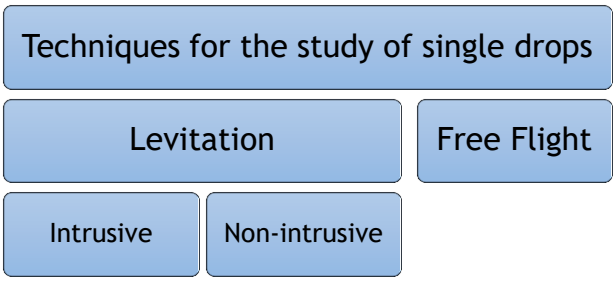

Figure 3.1. Techniques for the study of single drops

In free flight, the present case, the drops fall through the air and the different variables are measured by observation or by catching the drops at various heights. On the other hand, on levitation techniques the drops remain stationary, while the air flows past them.

Let us consider a jet discharged from a nozzle, in particular onwards from the point where it breaks into single individual drops due to inertial and aerodynamic forces. In order to determine the rate of heat and mass transfer from the drops, their velocity needs to be calculated. While along the horizontal axis, in the breaking point of the jet, the velocity's

component is negligible, the same cannot be said of its vertical component. Here it is assumed the drops equal their terminal velocity which will be used later on the Reynolds' number calculation.

The movement equation of a drop of d diameter, accordingly to Lapple and Sheperd (1940) is given by:

$$\frac{d\vec{U}}{d\tau} + \frac{3}{4}\frac{C_D}{d}\left(\frac{\rho_a}{\rho_w}\right)\left|\vec{U}\right|\vec{U} + \vec{g}\left(\frac{\rho_a}{\rho_w} - 1\right) = 0 \qquad (3.1)$$

At the terminal velocity in yy direction, with $\frac{d\vec{U}}{d\tau}$=0, U_y can be calculated with:

$$U_y = \sqrt{\frac{4dg(\rho_w - \rho_a)}{3\rho_a C_D}} \qquad (3.2)$$

For liquid droplets, the Reynols number can be evaluated from:

$$C_D = \frac{24}{Re} + \frac{6}{1+\sqrt{Re}} + 0.27,\ 1 < Re \leq 1000 \qquad (3.3\ a)$$

$$C_{D=} 0.6649 - 0.2712E^{-3}Re + 1.22E^{-7}Re^2 - 10.919E^{-12}Re^3,\ \&3600 \geq Re \geq 1000 \qquad (3.3\ b)$$

This model allows for the calculation of the heat and mass transfer maximum rates, however it does not take into account changes in temperature and air humidity as the drop falls.

The next parameter to take into account is the approach to be used in the calculation of the transfer rate of mass and heat: complete mixing model or non-mixing model. For complete mixing it is necessary to assume the drop's internal motion to be so powerful in order to reach complete mixing. In this case the temperature profile is planar and the only place where heat and mass transfer occur is at the drop's surface. On the other hand considering there's no mixing within the drop leads to the reduction of the energy equation to a problem in transient regime. The heat flow achieved if the first option is used is superior to the flow obtained through the second.

Strub *et al*, 2003 studied the freezing of a single water droplet, in particular the importance of evaporation on the overall freezing process and the impact of drops' size and velocity and air's humidity ratio and temperature on the crystallization phase.

The energy transport can be described by:

$$\rho_w C_p V \frac{dT_w}{d\tau} = -A[h_c(T_d - T_\infty) + h_d \rho_a h_{fg}(W_s - W_\infty) + \sigma e(T_d^4 - T_\infty^4)] \quad (3.4)$$

The left hand side of equation 3.4 represents the rate of energy change as the drop falls. The right hand side terms represent the transport of energy by convection, evaporation and radiation, respectively. The heat and mass transfer coefficients are constant.
The radiation may be determined with the introduction of the heat radiation term:

$$h_r = \sigma e(T_w^2 + T_\infty^2)(T_w + T_\infty) \quad (3.5)$$

The next step is to express the evaporation in term of temperature. Being the humidity saturation rate a function of temperature, a parabolic curve with the temperature as an independent variable may be used:

$$W_s = aT_w^2 + bT_w + c \quad (3.6)$$

Now passing from a single drop to a system, a water column with the shape of a cylinder will be considered as a representative model. An overall representation of the variables involved is presented in figure 3.2.

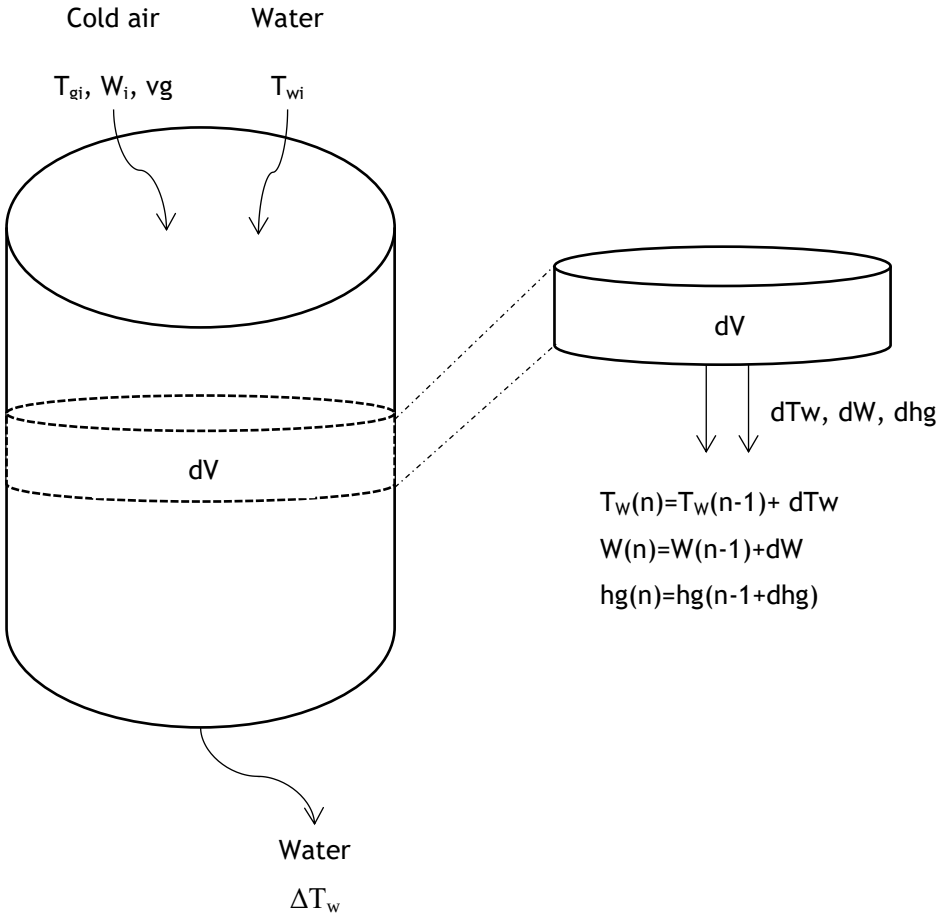

Figure 3.2. Heat and mass balance of a column of air in a differential element

Introducing the balance equation, from figure 3.2 as:

$$m_a dh = -[m_w - m_a(W + dW - W_i)]dh_f + m_a h_f dW \quad (3.7)$$

It can be simplified to:

$$m_a dh = -m_w dh_f + m_a h_f dW \quad (3.8)$$

The model starts by assuming a set of adequate initial conditions for the beginning of the calculation procedures. At this point values for the initial air and water temperatures, humidity ratio, drop diameter, air column height, flow ratio, air velocity and drop diameter are set.

A differential control volume is established to divide the water column in smaller portions in which the calculation procedure will be repeated until the bottom of the column is reached. This allows for a better accuracy of the results. For instance if a greater accuracy is desired, smaller step sizes, meaning a greater number of control volumes can be used.

The change of energy in the water, within the control volume is due to the heat and mass convection from the drops:

$$-m_w dh_f = h_c A_v dV(T_w - T_a) + \rho_a h_d A_v dV(W_s - W)h_{fg} \quad (3.9)$$

The left hand side of the above equation represents the energy change in the water, while the right hand side represents heat transfer due to convection and evaporation.

The change in the concentration of water vapor must equal the mass transfer in drops, or when W_S and W are the humidity ratios.

The heat and mass transfer coefficients calculated from the Ranz-Marshall relations are presented here in equations 3.10 and 3.11, according to Ranz *et al*, 1952:

$$Nu = \frac{h_0 d}{K_g} = 2 + 0.6 Re_d^{1/2} Pr_d^{1/3} \quad (3.10)$$

$$Sh = \frac{h_m d}{D_{vg}} = 2 + 0.6 Re_d^{1/2} Sc_d^{1/3} \quad (3.11)$$

Tang *et al* 1993 presented a document, in which they show a one-dimensional numerical model for liquid and solid drops in free-fall. In this document, a review of previews studies around the Ranz-Marshall relations is presented.
The Sherwood number for mass transfer is analogous to the Nusselt number for convective heat transfer.
The Schmidt number as the same relation between mass and momentum as the Prandtl between momentum and heat Hines and Maddox (1985).
In order to reach the desired coefficients, the Reynolds, Prandtl and Schmidt numbers are calculated according to equations 3.12 to 3.14.

$$Re = \frac{v_r.d}{\nu} \tag{3.12}$$

$$Pr = \frac{\nu}{\alpha} \tag{3.13}$$

$$Sc = \frac{\nu}{D} \tag{3.14}$$

The thermal diffusivity, viscous diffusivity, mass diffusivity and thermal conductivity are calculated according to Ashrae, 1977:

$$\alpha = \frac{1}{57736-585.78\mathrm{T_a}} \tag{3.15}$$

$$\nu = \frac{1}{80711.7-766.15\mathrm{T_a}} \tag{3.16}$$

$$\mathrm{D} = 2.227 \times 10^{-5}\left(\frac{\mathrm{T_a}+273}{273}\right)^{1.81} \tag{3.17}$$

$$\mathrm{k} = 0.024577 + 9.027 \times 10^{-5}\mathrm{T_a} \tag{3.18}$$

Now let us determine The Lewis number, which relates the convective heat transfer with the convective mass transfer to the water:

$$Le = \frac{h_c}{\rho_a C_{p,a} h_d} \cong \left(\frac{\alpha}{D}\right)^{2/3} \tag{3.19}$$

With the Lewis' number introduction, equation 3.9 is transformed into:

$$-m_w dh_f = \rho_a h_d A_V dV[LeC_{p,a}(T_w - T_a) + (W_s - W)h_{fg}] \tag{3.20}$$

And the specific heat in the definition of enthalpy to the flow:

$$h = C_{p,a}T_a + 2501W \tag{3.21}$$

The next step is to calculate the variation in the humidity ratio across a control volume which is given by:

$$m_a dW = \rho_a h_d A_v dV(W_s - W) \tag{3.22}$$

And the saturation humidity:

$$\mathrm{W_s} = 0.003894\mathrm{e}^{0.094442\mathrm{T_w}} \tag{3.23}$$

Finally:

$$\frac{dh}{dW} = Le\frac{(h_S - h)}{(W_S - W)} + (h_g - 2501Le) \tag{3.24}$$

Equation 3.24 represents the changes of state, in enthalpy variation as the drop goes through the air column, making possible for the calculation of the temperature variation:

$$\Delta T_W = -\frac{m_a}{m_w C_p}(\Delta h - h_f \Delta W) \tag{3.25}$$

Then the humidity ratio, the enthalpy of the air stream and the temperature of the water are incremented for the determination of the conditions on the other side of a control volume until the bottom of the column is reached. This value can be confirmed through a balance to the entire water column, represented by:

$$m_a h_{ai} + m_w h_{f,i} = m_a h_{ao} + [m_w - m_a(W_o - W_i)]h_{f,o} \tag{3.26}$$

If the air temperature is known, the mean mass transfer coefficient, $h_d A_V$, is known, the volume of air is:

$$V = \frac{m_a}{h_d A_V}\int_{W_i}^{W_0}\frac{dW}{W_s - W} \tag{3.27}$$

This model for a system of drops allows, as for the single drop case, for the calculation of maximum heat and mass transfer rates and takes into account changes in temperature and humidity ratio as the drop falls. However as studied by Yao *et al* 1976, vibrations and deformations of the falling drops have an impact on heat and mass transfer coefficients' values. The model here described in section 3.1. is summarized and presented in graphic form in figure 3.3

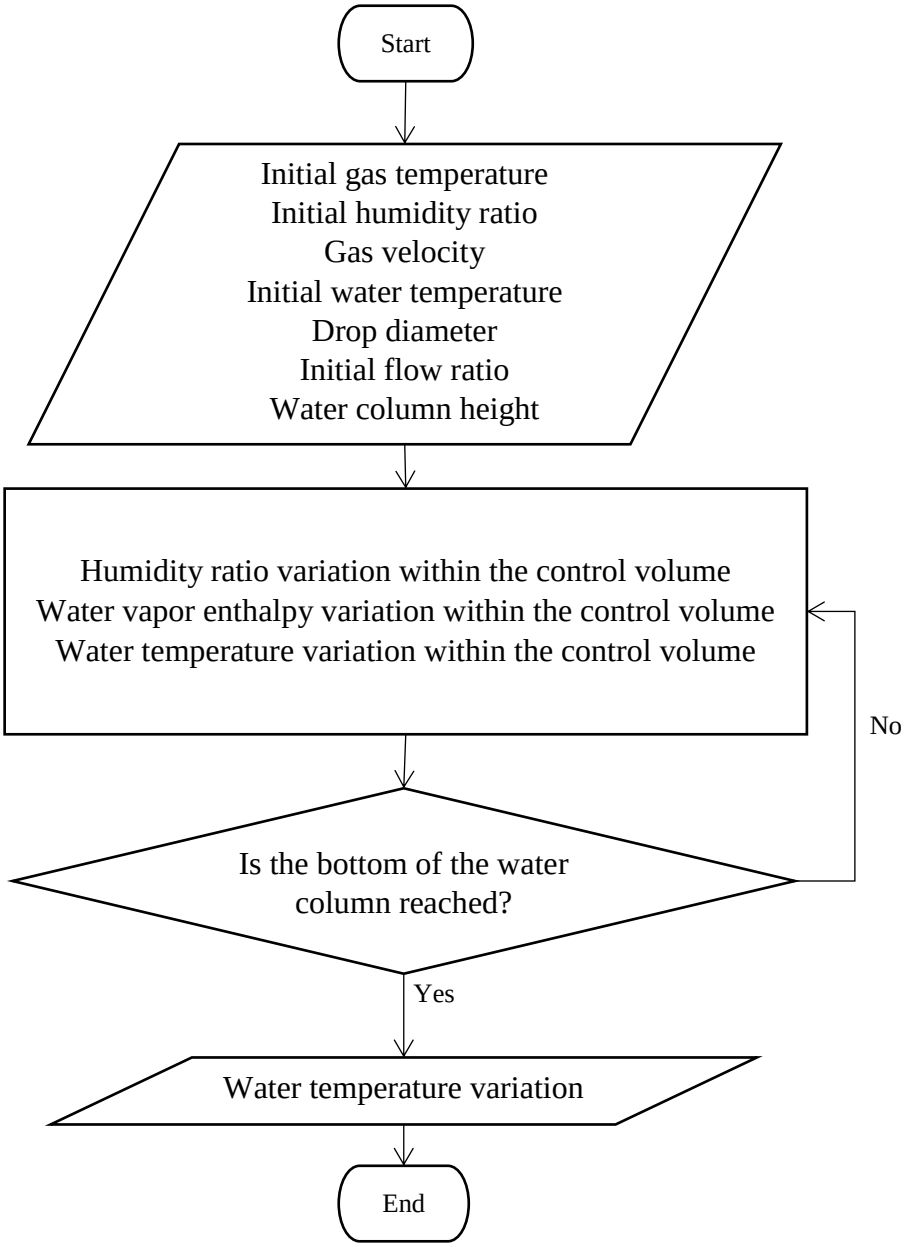

Figure 3.3. Flowchart for the calculation of the rate of cooling of a system of drops in free fall

Since both the non-mixing and the complete mixing model represent extreme situations, a correction factor which accounts for such distortions and vibrations, giving a solution in closer agreement with the experimental data was developed and is here present in equation 3.28.

$$g = 25\left(\frac{x}{d}\right)^{-0.7} \tag{3.28}$$

The correction factor developed approximates the complete mixing model with the experimental data for drops of water from 3 up to 6 mm in diameter for a ratio of x/d up to 600. Then, it is used along with the Ranz-Marshall relations already presented in equations 3.10 and 3.11, for a more realistic calculation of the heat and mass transfer coefficients.

$$\mathrm{Nu} = 2 + 15\mathrm{Re}_d^{1/2}\mathrm{Pr}_d^{1/3}\left(\frac{x}{d}\right)^{-0.7} \tag{3.29}$$

$$\mathrm{Sh} = 2 + 15\mathrm{Re}_d^{1/2}\mathrm{Sc}_d^{1/3}\left(\frac{x}{d}\right)^{-0.7} \tag{3.30}$$

3.3. Four phase freezing with supercooling

Previous studies, Hallet (1964), have devoted themselves to the search of a relation between the ice crystal structure, the rate of supercooling and the nucleation method. Various methods were tried over the years, such as polarized light in ice tunnels, at known conditions of size distribution and supercooling. From these researches comes an expression to the calculation of the water to ice ratio:

$$\int_0^{\Delta T} \frac{\sigma_T dT}{L_T} \tag{3.31}$$

For the development of a numerical model, each phase of the freezing process needs to be described individually. The prediction of the phase change temperature of each phase was achieved through the droplet's internal energy and heat losses to the environment. A scheme of the physical processes and main assumptions of the numerical model is presented in figure 3.4.

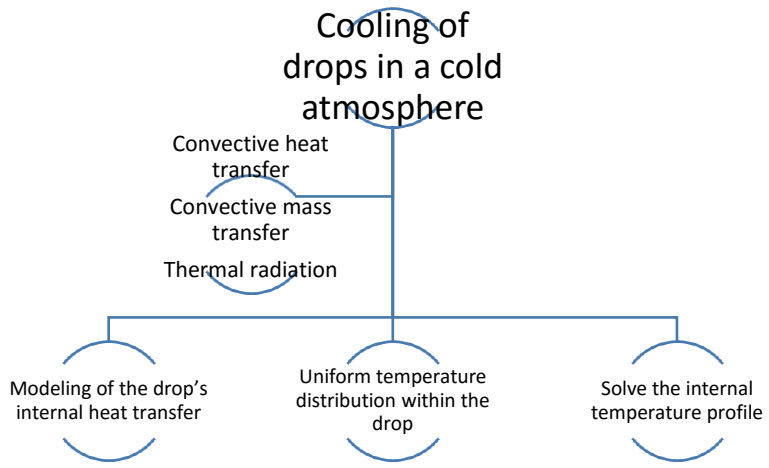

Figure 3.4. Main factors of the numerical solution

An energy balance is enough for the modeling of the freezing stage, through the external heat transfer and the amount of latent heat to be removed for the complete freezing of the mass of water within the drop.

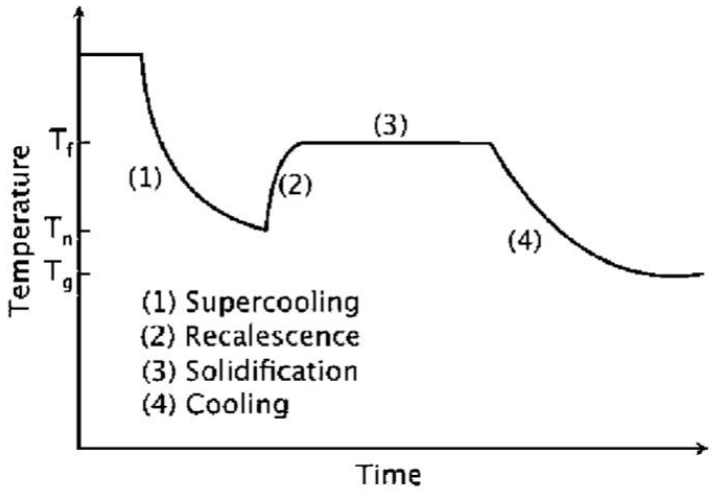

Figure 3.5. Generic representation of a four phase freezing process, Hindmarsh et al 2003 and Tanner et al 2011

This physical representation of a phase change process is composed by a supercooling period, where the temperature drops below T_f, followed by a recalescence stage, then a crystal growth phase and for last a cooling stage. Let us then discuss in a more detailed manner what physical processes are involved in each stage accordingly to figure 3.5.

I. Supercooling: the liquid drop is frozen from its initial temperature to the nucleation temperature (T_n), that lies below the equilibrium freezing temperature (T_f)
II. Recalescence: the supercooling stage induces a rapid kinetic growth of the crystal, with the release of latent heat, which results in a temperature increase until it reaches the equilibrium temperature
III. Solidification or freezing: the crystal growth happens at a constant equilibrium freezing temperature, until the droplet is completely solidified
IV. Cooling or tempering: the solidified drop freezes until it reaches the ambient temperature

The cooling of the solid particles in stages I and IV is determined by the energy exchange between the particles themselves and the environment. The internal temperature profile can be solved through a description between the transient heat transfer equations, with the help of appropriate boundary conditions. The heat transfer in stage III is a Stefan typical problem, which as described in the introductory chapter, consists in determining the temperature distribution and the interface's location.

Translating the text into mathematical language, it is known for a uniform temperature distribution the rate of temperature change is given by:

$$\rho_d V_d C_{pd} \frac{dT_d}{dt} = -S_d(q_h + q_m + q_r) \quad (3.32)$$

Where q_h is set accordingly to Newton's cooling law: $q_h = h_0(T_d - T_g)$ and q_m from:

$$q_m = Lh_m(\rho_v - \rho_g) \quad (3.33)$$

The convective coefficients once again arise from the Ranz-Marshall relations already explained through equations 3.10 and 3.11.

For last, the thermal flux due to radiation is achieved with the Stefan-Boltzmann fourth power law: $q_r = \varepsilon\sigma(T_d^4 - T_g^4)$ (3.34)

As seen through figure 3.6, a drop with initial supercooling, after the nucleation stage suffers a temperature increase until it reaches T_f. During this stage, which is recalescence, there is a percentage of volume that solidifies - V_f.

$$V_f = V_d \frac{\rho_d C_{pd}(T_f T_n)}{\rho_s L_f} \quad (3.35)$$

Since the gas temperature at the surface is usually different from the mean value, it is possible to account this discrepancy with the correction of two thirds the mean temperature:

$$T = \frac{T_g + 2T_d}{3} \quad (3.36)$$

The dimensionless groups- the Reynolds, Prandtl and Schmidt numbers – depend on the properties of the gas (μ_g, K_g and D_{vg}),, which in turn depend on the temperature of the surrounding gas. In order to accommodate these variations, it is possible to make use of the Sutherland relations:

$$\mu_g(T) = \frac{A_1 * T^{1.5}}{T A_2} \quad (3.37)$$

$$K_g = \frac{K_1 * T^{1.5}}{T * K_2} \quad (3.38)$$

With:

Table 3.1. Constants of the Sutherland relations

Dynamic viscosity	Thermal conductivity
A_1=1.457E-5	K_1=252
A_2=110;	K_2=200

It is also assumed the drop's temperature variation is instantaneous, therefore neglecting the recalescence time.

After the nucleation stage, the cooling of the remaining liquid is controlled by the heat transfer from the drop to the gas at a certain T_f. Here it is assumed the nucleation is uniform throughout the drop.

With the incorporation of equation 3.31 in the heat balance 3.32 comes:

$$\rho_d V_d C_{pd} \frac{dT_d}{dt} = -S_d(q_h + q_m + q_r) + L_f \rho_s \frac{dV_f}{dt} \tag{3.39}$$

If the temperature throughout the solidifying process remains constant, $\frac{dT_d}{dt} = 0$ and:

$$L_f \rho_s \frac{dV_f}{dt} = S_d(q_h + q_m + q_r) \tag{3.40}$$

In order for the mass transfer through evaporation to continue, there is a need to assume the drop's exterior is liquid, in this process. If one is to assume the outer surface is solid, the mass transfer is by sublimation.

Lastly, the uniform temperature hypothesis within a drop is only valid if Bi≤0.1. Bi represents the Biot number (equation 3.41) and for values above 0.1, it is not possible to ignore internal temperature gradients.

$$Bi = \frac{h_o d}{2K_d} \tag{3.41}$$

The low level of crystal growth can happen during heat transfer after recalescence. From here, the crystal formed during recalescence has a major impact in the final structure, due to the low volume of liquid within the drop, Tanner *et al* (2011).

A big supercooling level during nucleation will lead to a larger frozen fraction of water at recalescence. Thus contributing to a larger percentage of the microstructure being formed at this stage.

On the other hand, there are many materials which do not exhibit supercooling, therefore neither will they present a recalescence stage. Once the freezing temperature, T_f, is reached, the nucleation and crystallization stages begin. The release of latent heat is slow enough for a decrease of the droplet freezing rate to occur instead of a temperature increase. This new model will only be comprised of three stages:

I. Initial cooling of the liquid
II. Solidification or crystallization
III. Cooling of the solid droplet

Usually, radiation is not an issue when discussing spray freezing, neither is the mass flux, due to the droplets being small enough and freeze instantaneously. Therefore, the thermal radiation, q_r, and the mass heat flux, q_m, can be neglected.
The cooling of the liquid and the solid (I and III) is fully described through a convective heat transfer process.
Once the droplet reaches its freezing temperature, T_f, the crystallization process begins. Here it's assumed the drop starts solidifying inwards. The beginning of this stage is characterized by a rapid variation of the drop cooling rate, which has the final consequence of a smoother cooling line.
The governing equation for the three stage model is:

$$\rho_d V_d C_{p\gamma} \frac{dT_d}{dt} = -S_d * h_0\left(T_d - T_g\right) + L_f \rho_d \frac{dV_f}{dt} \quad (3.42)$$

With

$$C_{p\gamma} = (1-\gamma)C_{pl} + \gamma C_{ps} \quad (3.43)$$

$$\gamma = \frac{T_f - T_d}{T_f - T_s} \quad (3.44)$$

Where:

C_{pl}=2.2 KJ/KgK

C_{ps}=1.25 KJ/KgK

In order to express dV_f/dt, a new correlation is needed:

$$d_1 = (1-\gamma)d \quad (3.45)$$

Since the droplet freezes inward, the freezing volume is:

$$V_f = \frac{\pi d^3}{6}[1-(1-\gamma)^3] \quad (3.46)$$

For last, we have:

$$\rho_d * d\left[C_{p\gamma} + 3L_f * \frac{(1-\gamma)^2}{T_f - T_s}\right] * \frac{dT_d}{dt} = -6h_0(T_d - T_g) \quad (3.47)$$

Equation 2.41 is used for the calculation of the droplet's temperature, T_d. The factors γ and $C_{p\gamma}$ depend on T_d.

3.4. Initial conditions and flow configuration

In this section the initial conditions for the numerical simulations will be set. Figure 3.6 represents the flow configuration where water drops with diameters of 3, 4, 5 and 6 mm will be injected. The injector is set to the center of the cross section as represented in the figure. The tunnel has a cross section of 170x170 mm per 1000 mm on the vertical axis. The velocity of the air corresponds to 3 cm/s and the flow mass ratio of water/air is set to 0,1 Kg.
The value of both drops and water temperature varies slightly from one simulation to the next, according to the humidity ratio they are subjected to, as seen in table 3.2. However the ambient temperature will be kept constant during each simulation to maintain a first order phase transition as previously explained on chapter 2.

Table 3.2. Values for drop diameter, initial drop temperature, air temperature and humidity ratio

Drop diameter [mm]	Initial drop temperature [°C]	Air temperature [°C]	Humidity ratio
3	40.70	23.29	0.29
3	40.73	22.31	0.36
3	40.69	23.33	1.00
4	40.74	22.44	0.36
4	40.64	21.33	0.52
4	40.79	23.33	1.00
5	40.68	22.88	0.29
5	40.72	22.56	0.36
5	40.74	23.61	1.00
6	40.74	22.14	0.36
6	40.66	21.33	0.52
6	40.70	23.33	1.00

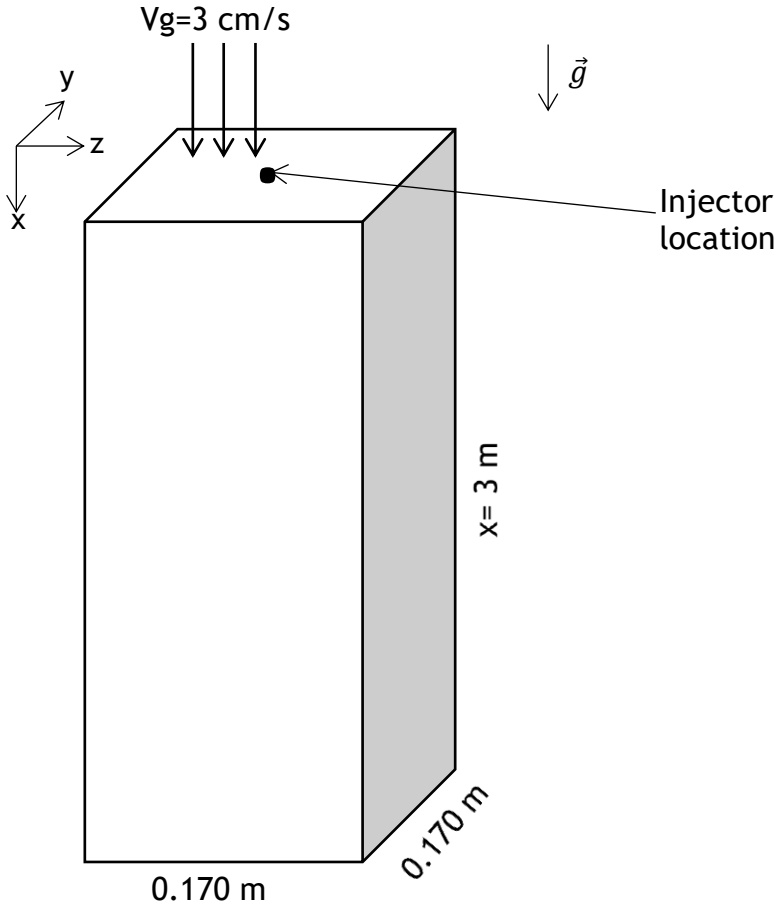

Figure 3.6. Computational domain

4. Results and Discussion

4.1. Introduction

The mathematical model previously described on section 3.1 was implemented in order to evaluate the rate of cooling of drops in free fall. Several simulations were carried out for a range of values of drop diameters and humidity ratios, according to the experiments of Yao and Schrock (1976). Simulations were carried out for drops with diameters of 3, 4, 5 and 6 mm and humidity ratios of 0.29, 0.36, 0.52 and 1. Section 4.2 presents the numerical study for the variation of drops' diameter and its influence on the overall freezing process. On the other hand section 4.3 focuses on the humidity ratio variation.
Lastly this chapter concludes with a brief summary.

4.2. Influence of variable drop diameter on the freezing process

A comparison between the Ranz-Marshall relations in their original formulation, as presented by Ranz and Marshall (1952), also described in this document on equations 3.10 and 3.11 and their corrected formulation – to attempt to account for vibrations and deformations – as established by Yao and Schrock (1976) and here previously explained on equations 3.29 and 3.30 is performed in order to try to establish differences between the two modulations and in which conditions one can be used in favor of the other. Also, the complete falling distance as defined in the correction factor on equation 3.28 is established as 3 m and the velocity of the air stream is set to 3 cm/s.
For every figure in the present section filled circles correspond to the experimental data, while hollow circles represent predictions, being the dashed line relative to the classical Ranz-Marshall relations while the solid one relate to the Ranz-Marshall equations adding the correction factor
The results are presented as dimensionless quantities. The drops' temperature variation, on the vertical axis, is divided by their own initial temperature while on the horizontal axis, the total falling distance is divided by the drops own diameter.
The number of control volumes is set to 30 so it happens each volume represents 0.1 m of the column.

Figure 4.1 represents the variation on drops' temperature falling through the air for a diameter of 3 mm and humidity ratio of 0.36. The drops' temperature variation corresponds to the oscillation on the entire column as previously defined. For a diameter of 3 mm and humidity ratio of 0.36 the complete mixing model over predicts cooling for falling distances greater than 50 diameters, while the mixing model under predicts cooling for falling distances lower than 350 diameters. The predictions suggest early steady state conditions, while for x/d > 350 the effects of distortions and vibrations become predominant.

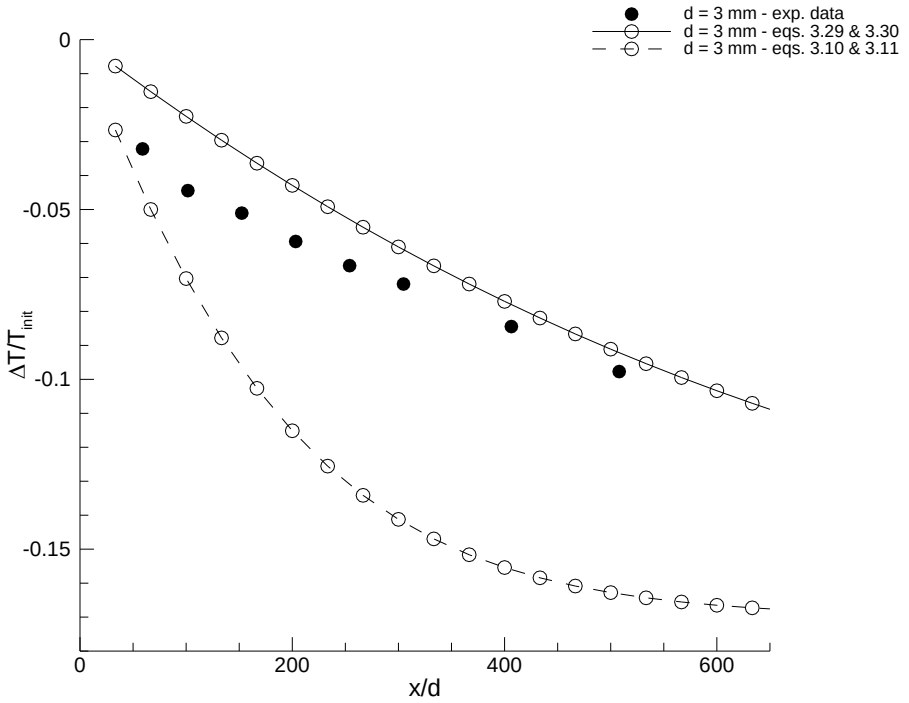

Figure 4.1. Variation on drops' temperature falling through the air for a diameter of 3 mm and humidity ratio of 0.36

Figure 4.2 shows the temperature variation for drops falling through the air for a humidity ratio of 0.36 and diameters of 3, 4, 5 and 6 mm. Besides, on table 4.1 the values for the drops' initial temperature and the constant air temperature are also presented.

The results show the complete mixing model predictions are in agreement for falling distances lower than 50 diameters. For this region cooling may be considered steady state and independent of diameter Otherwise, the results suggest the effects of distortions and vibrations in the falling drops are heavily dependent on drop size. Effects of distortions and vibrations in the falling drops become predominant early as diameter values increase, e.g. for a diameter of 6 mm the effects of distortions and vibrations in the falling drops become predominant x/d > 100.

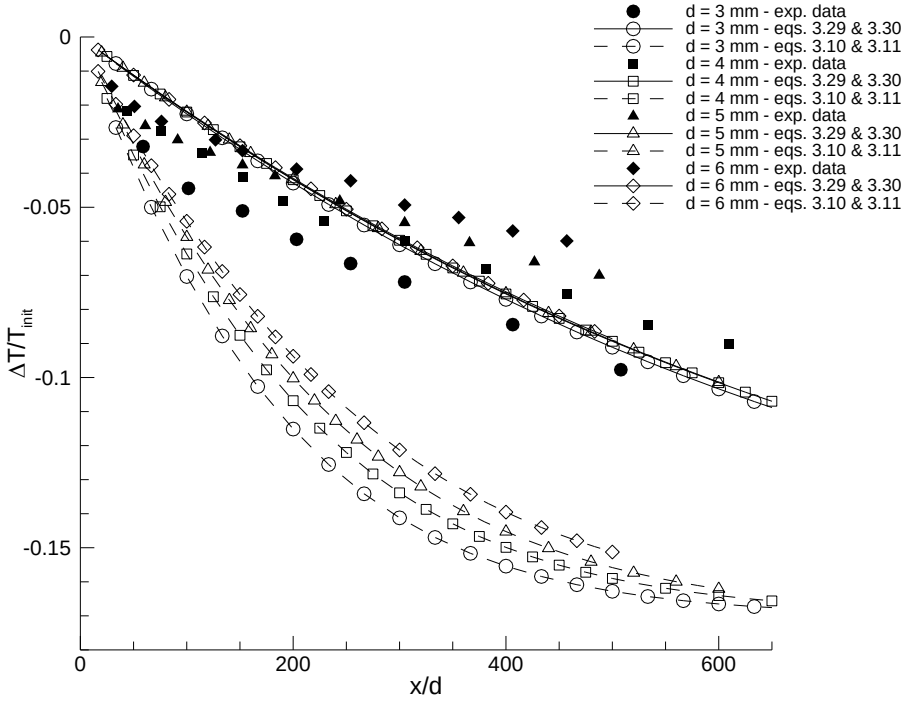

Figure 4.2. Variation on drops' temperature falling through the air for variable drop diameter and humidity ratio of 0.36

Table 4.1. Initial properties for the simulation of a humidity ratio 0f 0.36

Drop diameter [mm]	Initial drop temperature [ºC]	Air temperature [ºC]	Humidity ratio
3	40.73	22.31	0.36
4	40.74	22.44	0.36
5	40.72	22.56	0.36
6	40.74	22.14	0.36

Figure 4.3 shows the drops' temperature variations for a humidity ratio of 0.29 and diameters of 3 and 5 mm. Through this figure analysis, it is seen the experimental data is better approximated by the complete mixing model given by equations 3.10 and 3.11, especially for values of less than 100 diameters, in the case of 3 mm drops, while for the case of 5 mm drops, overall the complete mixing model is a good approximation. In this case, the range of temperatures used is expressed on table 4.2 for each of the diameter values tested.

Table 4.2. Initial properties for the simulation of a humidity ratio 0f 0.36

Drop diameter [mm]	Initial drop temperature [ºC]	Air temperature [ºC]	Humidity ratio
3	40.70	23.29	0.29
5	40.68	22.88	0.29

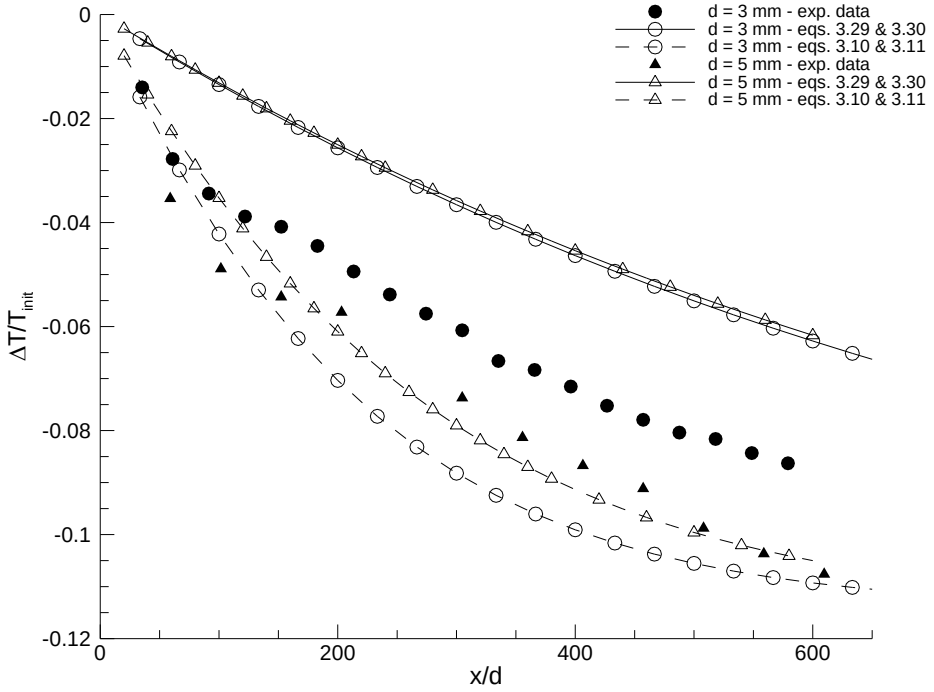

Figure 4.3. Variation on drops' temperature falling through the air for variable drop diameter and humidity ratio of 0.29

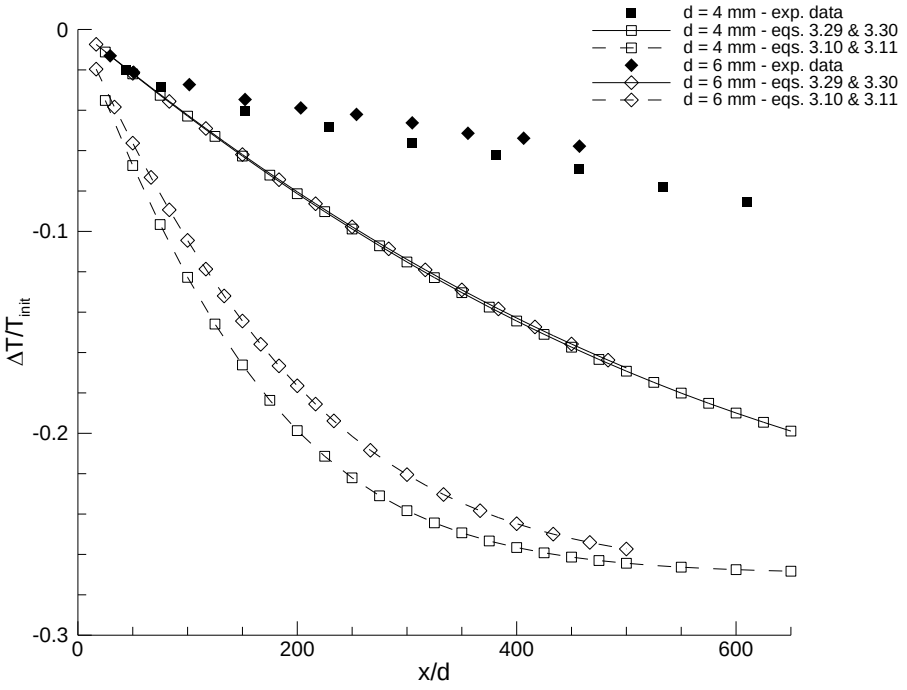

Figure 4.4. Variation on drops' temperature falling through the air for variable drop diameter and humidity ratio of 0.52

Figure 4.4 shows the drops' temperature variations for a humidity ratio of 0.52 and diameters of 4 and 6 mm. In this figure, the mixing model proves to be an effective approximation only for values of less than 80 diameters, hinting cooling in this conjugation of values may be a problem on a transient regime and the non-mixing model may be needed for a better approach. This is of greater relevance if we take into account figure 4.5 for a humidity ratio of 1, where the mixing model completely fails in approximating the experimental data. The initial properties for both the cases of humidity ratios of 0.52 and 1 are presented on tables 4.3 and 4.4 respectively.

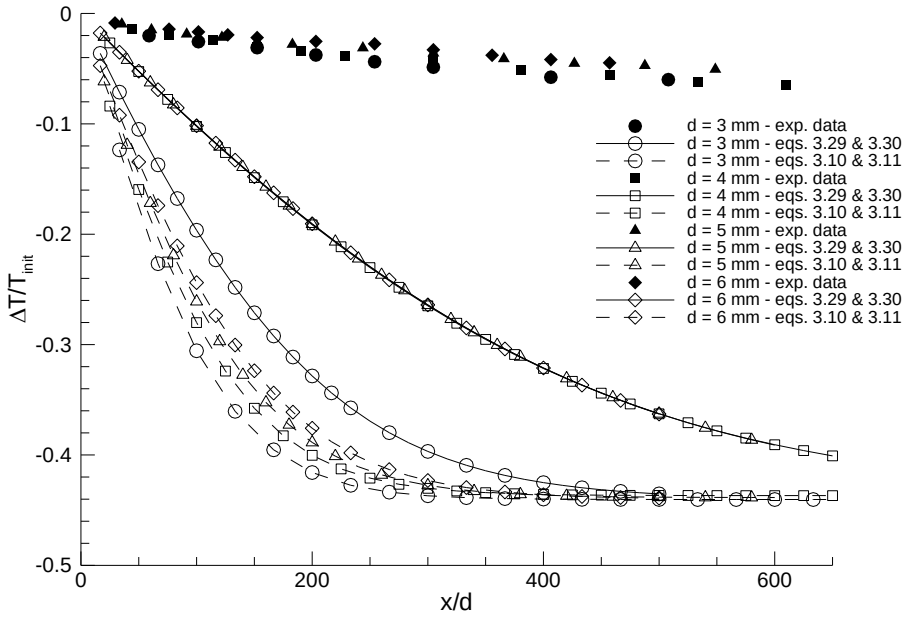

Figure 4.5. Variation on drops' temperature falling through the air for variable drop diameter and humidity ratio of 1.

Table 4.3. Initial properties for the simulation of a humidity ratio 0f 0.52

Drop diameter [mm]	Initial drop temperature [ºC]	Air temperature [ºC]	Humidity ratio
4	40.64	21.33	0.52
6	40.66	21.33	0.52

Table 4.4. Initial properties for the simulation of a humidity ratio 0f 1

Drop diameter [mm]	Initial drop temperature [ºC]	Air temperature [ºC]	Humidity ratio
3	40.69	23.33	1.00
4	40.79	23.33	1.00
5	40.74	23.61	1.00
6	40.70	23.33	1.00

4.3. Influence of variable humidity ratio on the freezing process

In this section the results for the simulations of variable humidity ratios are presented.

Once again for figure in the present section filled circles correspond to the experimental data, while hollow circles represent predictions, being the dashed line relative to the classical Ranz-Marshall relations while the solid one relate to the Ranz-Marshall equations adding the correction factor

The results are presented as dimensionless quantities. The drops' temperature variation, on the vertical axis, is divided by their own initial temperature while on the horizontal axis, the total falling distance is divided by the drops own diameter.

Figure 4.6 represents the variation on drops' temperature falling through the air for drops of diameter of 3 mm and humidity ratios of 0.29, 0.36 and 1. For the case of a humidity ratio of 1, neither the complete nor the mixing model proves to be effective in the modeling. Here clearly a transient regime is presented and the non-mixing model could be of use. The drops subject to ratios of 0.29 and 0.36 are in closer agreement with the experimental data. The values for both the ambient and air temperatures are present on table 4.5.

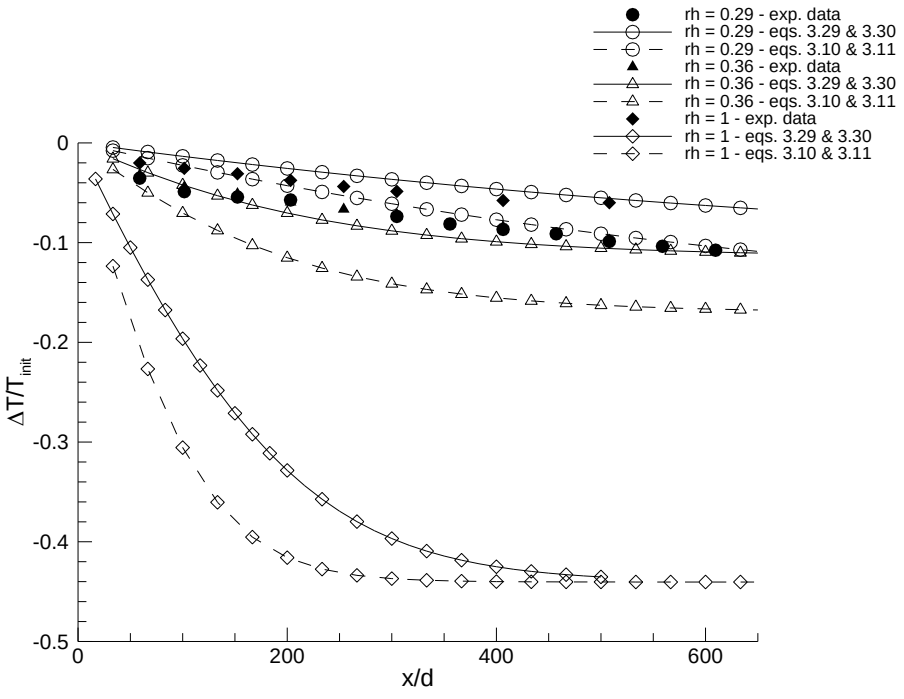

Figure 4.6. Variation on drops' temperature falling through the air for a diameter of 3 mm and variable humidity ratio

Table 4. 5. Initial properties for the simulation of a diameter of 3 mm

Drop diameter [mm]	Initial drop temperature [ºC]	Air temperature [ºC]	Humidity ratio
3	40.70	23.29	0.29
3	40.73	22.31	0.36
3	40.69	23.33	1.00

In figure 4.7 the temperature variation for drops of 4 mm in diameter falling through the air subject to humidity ratios of 0.36, 0.52 and 1 is presented. Once again drops subject to a ratio of 1 represent the biggest disparity between both the numerical and experimental data, while the ratio of 0.36 still represents the better approximation with the experiments. Now introducing a middle value for the humidity (0.52), it is seen through the figure analysis, the mixing model is effective up to 50 diameters, after which steady state regime leads to a transient one. Table 4.6 contains the values used for the temperature.

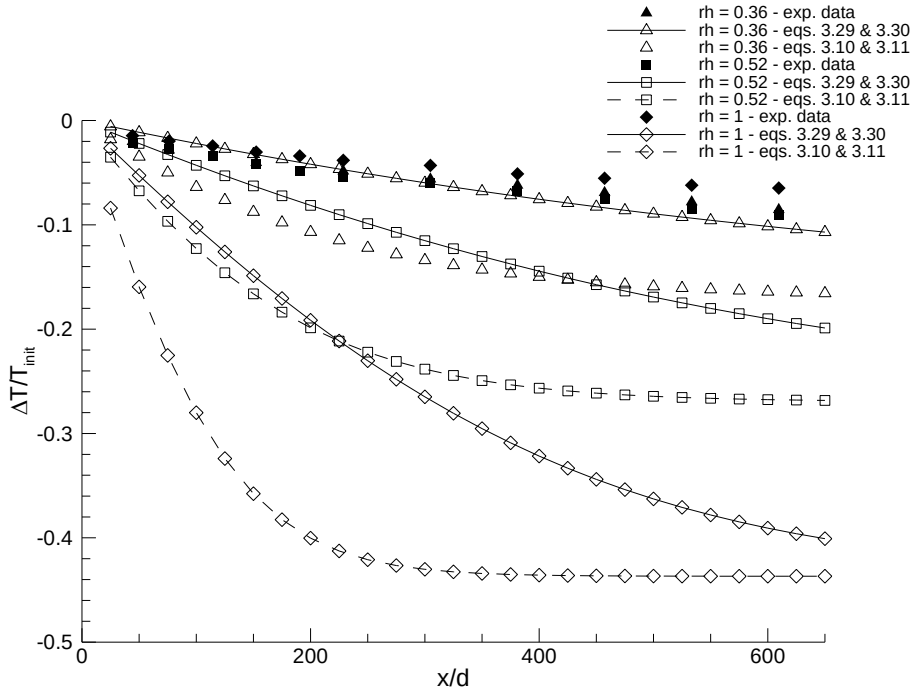

Figure 4.7. Variation on drops' temperature falling through the air for a diameter of 4 mm and variable humidity ratio

Table 4.6. Initial properties for the simulation of a diameter of 4 mm

Drop diameter [mm]	Initial drop temperature [ºC]	Air temperature [ºC]	Humidity ratio
4	40.74	22.44	0.36
4	40.64	21.33	0.52
4	40.79	23.33	1.00

In figure 4.8 are presented the numerical data obtained through numerical simulation for drops with 5 mm diameter and variable humidity ratio of 0.29, 0.36 and 1. The complete and the mixing models continue to be ineffective in modelling drops under a humidity ratio of 1, while a ratio of 0.36 still is in closer agreement with the experiments. As for the 0.29 ratio differences between numerical and experimental data are presented. The complete mixing model under predicts cooling for more than 150 diameters, while the mixing model over predicts cooling. For this case, table 4.7 shows the values used for the temperatures.

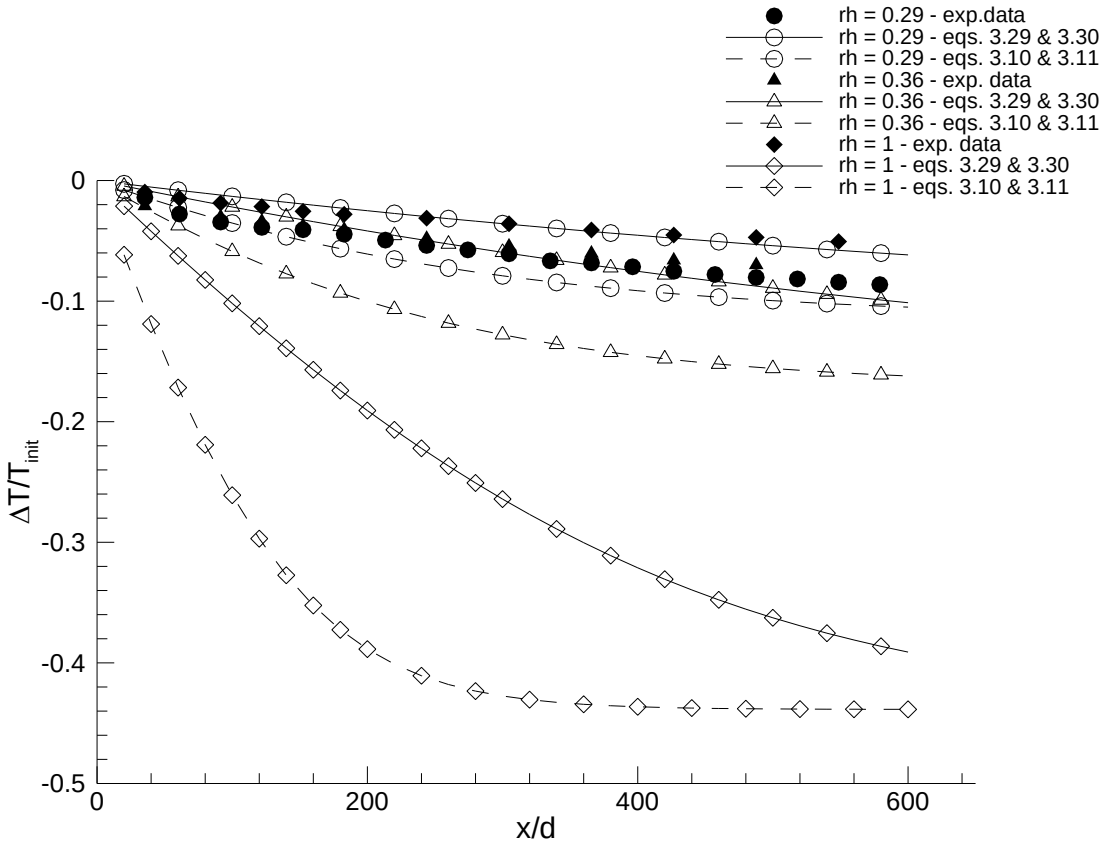

Figure 4.8. Variation on drops' temperature falling through the air for a diameter of 5 mm and variable humidity ratio

Table 4.7. Initial properties for the simulation of a diameter of 5 mm

Drop diameter [mm]	Initial drop temperature [ºC]	Air temperature [ºC]	Humidity ratio
5	40.68	22.88	0.29
5	40.72	22.56	0.36
5	40.74	23.61	1.00

In figure 4.9 drops of diameter 6 mm and humidity ratio of 0.36, 0.52 and 1 are presented. Overall the behavior reflects that of the previous figures. In this case both the mixing and complete mixing models are ineffective in modelling the experimental data for humidity ratios of 0.52 and 1, while for the ratio of 0.36 the mixing model is a good approximation. The range of temperatures used for these simulations is presented on table 4.8.

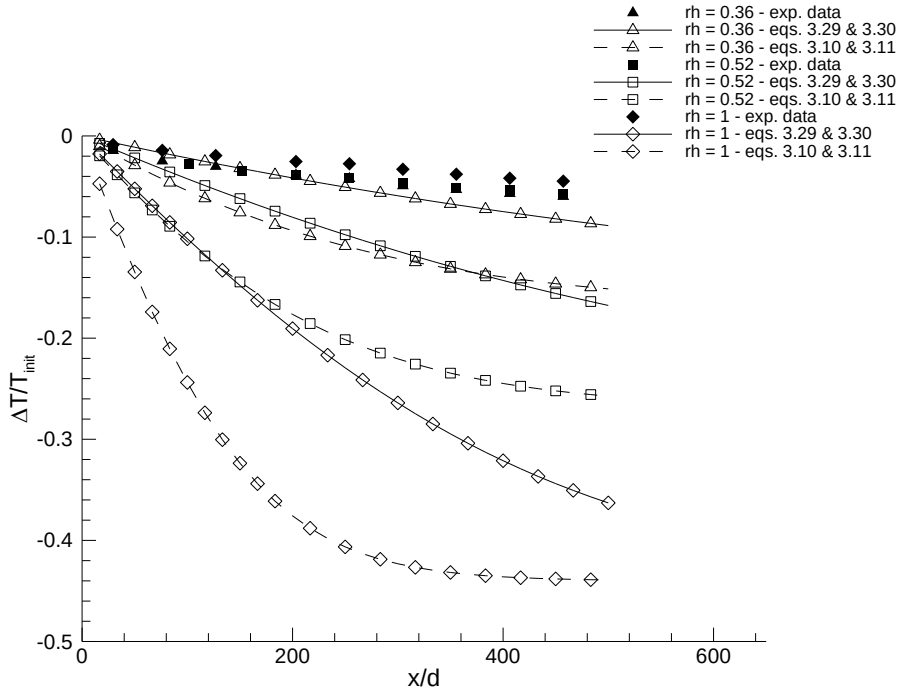

Figure 4.9. Variation on drops' temperature falling through the air for a diameter of 6 mm and variable humidity ratio

Table 4.8. Initial properties for the simulation of a diameter of 6 mm

Drop diameter [mm]	Initial drop temperature [ºC]	Air temperature [ºC]	Humidity ratio
6	40.74	22.14	0.36
6	40.66	21.33	0.52
6	40.70	23.33	1.00

The mixing model is able to model in a good agreement with experimental data drops subject to a middle value for humidity, around 0.36, around which steady state regime is encountered. An increase in humidity's values leads to an over prediction on the cooling of drops by this model and to the presence of transient regime. On the other hand, a decrease in humidity levels will lead to an under prediction of drops' cooling and steady state regime.

4.3. Summary

In this chapter the results were presented regarding the study freely falling water droplets for a range drops' diameters and humidity ratios. The predictions were compared with the available experimental data; first for the influence of variable drops' diameter and later for the influence of variable humidity ratio. The results are in part presented in Magalhães *et al* (2016) (see attachments 1 and 2), regarding the influence of diameter variation on the overall freezing process.

5. Conclusions and future work

In this section are presented the conclusions of the research carried out on the subject of freezing of a liquid as well as the possible outcomes in respect to which works it can lead in the future.

Numerical simulations were carried out for the case of a system of water drops in free fall under several humidity conditions and for different values of drops' diameters, in which it was possible to evaluate humidity's influence on the overall freezing process. During our simulations, differences were found between the numerical data obtained through simulation and experimental data. A possible explanation lies with the fact modeling droplets in free fall may present itself a far more complex problem that it was initially considered. For example vibrations and distortions may influence the droplet's heat and mass transfer rates in a greater measure. We attempted with the use of the empirical factor g to account for this phenomenon, however a more detailed modeling, with the incorporation of oscillation amplitudes into the Reynolds number could be of use, given the fact the numerical data better approximates experiments for a middle level humidity ratio.

In a concluding remark, future studies could focus on the study on a two way coupling perspective, in the influence of the droplets on turbulence, as the increasing of particles mass-loading ratio will makes this relevant

6. References

Anderson JR, J. D. (1995) *Computational Fluid Dynamics: The Basics With Applications*, McGraw-Hill Book Co.

Alexiades, V. and Solomon, A. (1993) *Mathematical Modeling of Melting and Freezing Processes*, Hemisphere Publishing, Washington DC

Ashrae (1977) *Handbook of fundamentals*, American Society of Heating, Refrigerating and Air Conditioning Engineers

Caginalp, O. and Socolovsky, E. (1991) *Computation of sharp phase by spreading: The planar and spherically symmetric cases*, J. Comp. Phys., 95, pages 85-100

Caliskan, F. and Hajiyev, C. (2013). *A review of in-flight detection and identification of aircraft icing and reconfigurable control*, Istanbul Technical University, Progress in Aerospace Sciences 60, 12-34

Coker, A. C. (1995) *FORTRAN programs for Chemical Process Design, Analysis and Simulation*, Elsevier Science & Technology Books

Cao, Y. and Wu, Z. (2014). *Aircraft Flight Characteristics in Icing condition*, University of Beijing, Progress in Aerospace Sciences 74 62-80

Dickinson, D. R. and Marshall, W. R. (1968) *The rates of evaporating of sprays*, Journal of the american institute of chemical engineers, vol. 14, no 4, 541-552

Dillingham, L. (2010). *Aviation safety, preliminary information on aircraft icing and winter operations, GAO, United States Government Accountability Office testimony before the subcommittee on aviation,* Committee on Transportation and Infrastructure

Fix, G. and Lin, J. (1988) *Numerical simulations of nonlinear phase transitions – I. The isotropic case*, Nonlinear Analysis, 12, page 811-823

Gao, W., Smith, D. W. and Sego, D. C. (2000) *Freezing Temperatures of Freely Falling Industrial Wastewater Droplets*, Journal of cold regions engineering, September,14:101-118

Glicki, N. V. and Mardonko, M. (1961) *Formation of monocrystalline granules of ice upon solidification of a supercooled drop of water*, Soviet Physics Doklady, 1145-1149

Griebel, M., Merz, W. and Neunhoffer, T. (1997) *Mathematical Modeling and Numerical Simulation of Freezing Processes of a Supercooled Melt under Considerations of Density changes*, International Journal of Numeric Methods, pages 281-301

Hallett, J. (1964) *Experimental Studies of the Crystallization of Supercooled* Water, Journal of Atmospheric Sciences, 21, pages 671-682

Hauk, T.,Bonaccurso, E., Roisman, I. V. and Tropea, C. (2015). *Ice crystal impact onto a dry solid wall. Particle fragmentation*, Proceddings of the Royal Society

Hindmarsh, J. P., Russell, A. B. and Chen, X. D. (2003) *Experimental and Numerical Analysis of the Temperature Transition of a Suspended Freezing Water Droplet*, International Journal of Heat and Mass Transfer 46, pages 1199-1213

Hindmarsh, J. P., Russell, A. B. and Chen, X. D. (2007) *Fundamentals of the Spray Freezing of Foods – microstructure of frozen droplets*, Journal of Food Engineering, 78, pages 136-150

Hines, A. L. and Maddox, R. N. (1985) *Mass Transfer: Fundamentals and Applications*, Prentice Hall

Hughes, R. R. and Gilliland, E. R. (1952) *The mechanisms of drops*, Chemical Engineering Progress, vol. 48, no. 10, p. 497-504

Lunardini, V. J. (1981) *Heat transfer in cold climates*, New York: Van Nostrand-Reinhold

Magalhães, L., Barata, J. a Silva, A. (2016) *Numerical study of freezing droplets*, CEM 2016, June 1-3

Patankar, (1980) S. V. *Numerical Heat Transfer and Fluid Flow*, Hemisphere Publishing

Phase field computations of single-needle crystals, crystal growth, and motion by mean curvature, SIAM J. Sci. Com., 15, page 106-126, 1994

Ranz, W. E. and Marshall, W. R. (1952). *Evaporation from drops*, Chemical Engineering Progress, vol.48, no 3 &4, 141-146, 173-180

Robinson, M. B. (1981) *Undercooling measurement in a low-gravity containerless environment*, Space Sciences Laboratory, NASA TM-82423

Smith, J. (1981) *Shape instabilities and pattern formation in solidification: A new method for numerical solution of the moving boundary problem*, J. Com. Phys., 39, page 112-127

Sethian, J. and Strain, J. (1992) *Crystal growth and dendritic solidification*, J. Com. Phys., 98, page 231-253

Shampine, L. F. and Thompson, R. J. *An Efficient Method for the Numerical Solution of One-Phase Stefan Problems*, Sandia Laboratories, Applied Mathematics Department, Albuquerque, New Mexico 87115

Strub, M., Jabbour, O. and Bédécarrats, J. P. (2003) *Experimental study and modelling of the crystallization of a water droplet*, International Journal of Refrigeration, 26, 59-68

Sullivan, J., Lynch, D. and O'Neil, K. (1987) *Finite element simulation of planar instabilities during solidification of an undercooled melt*, Journal of Computational Physics, 69, page 81-111

Tang, K. C. and Czys, R. R. (1994) *A one-dimensional numerical model for the computation of the transient temperature of liquid and solid drops in free-fall*, Illinois State Water Survey

Tanner, F. X. (2011) *Droplet Freezing and Solidification*, Handbook of Atomization and Sprays, Springer Science + Business Media

Temos, J., Pratt, H. R. C. and Stevens, G.W. (1996) *Mass Transfer to Freely-Moving Drops, Journal of Chemical Engineering Science*, Vol. 51, No. 1, pages 27-36

Yao, S. C. and Schrock, V. E. (1976) *Heat and mass transfer from freely falling drops*, Journal of heat transfer, ASME, vol. 98, no 1, 120-125

Zarling, J. P. (1980) *Heat and mass transfer from freely falling drops at low temperatures*, CRREL Report 80-18

Attachment 1 – Extended abstract accepted for the CEM 2016

NUMERICAL STUDY OF FREEZING DROPLETS

Magalhães, Leandro[1]; Barata, Jorge[2]; Silva, André[3]
[1] University of Beira Interior, Department of Aerospace Science, Portugal, leandrobmagalhaes@gmail.com
[2] University of Beira Interior, Department of Aerospace Science, Portugal, jbarata@ubi.pt
[3] University of Beira Interior, Department of Aerospace Science, Portugal, andre@ubi.pt

KEYWORDS: *heat and mass transfer, Ranz-Marshall relations, humidity ratio*

ABSTRACT: The present work is devoted to the numerical study of freezing processes which have become of major importance in aeronautical engineering. According to Caliskan and Hajiyev (2013), the most common causes of structural damage to aircrafts due to climacteric changes are the result of lightning strikes and icing at the wing's leading edge or empennage. The icing of a wing's leading edge turns the smooth airflow over the wing into a turbulent one, decreasing lift and increasing drag. At temperatures below zero, icing spreads to the trailing edge, affecting a greater percentage of the wing. Overall, icing has a negative effect on an aircraft's aerodynamic performance, especially during take-off and landing and anti-icing systems on modern aircrafts make use of heat exhausted from the engines, to prevent the ice from forming, which increases fuel consumption and in turn the operational costs of the aircraft. Several authors, Yao and Schrock (1976) and Zarling (1980), have studied heat and mass transfer on freely-falling drops, in order to determine its rate of cooling under several humidity conditions, making use of the Ranz-Marshall relations for the Nusselt and Sherwood numbers. This model allows to calculate the heat and mass transfer maximum rates, however it does not take into account changes in temperature and air humidity as the drop falls. It is necessary to assume the drop internal movement be powerful enough, so that complete mix occurs – the temperature profile is planar and the heat and mass transfer happens only at the drop's surface – or there isn't mix in the drop, so the energy equation is reduced to a heat transfer problem in transient regime. The objective of the present work is to investigate numerically the freezing of free falling droplets for different diameters and air humidity. The predictions are compared with experimental data and the numerical analysis is conducted to provide insight into the heat transfer involved in the freezing process under several humidity conditions.

REFERENCES

[1] F. Caliskan and C. Hajiyev, *A review of in-flight detection and identification of aircraft icing and reconfigurable control*, Istanbul Technical University, Progress in Aerospace Sciences 60 (2013), 12-34

[2] Yao, S. C. and V. E. Schrock, *Heat and mass transfer from freely falling drops*, Journal of heat transfer, ASME, vol. 98, no 1, 120-125, 1976

[3] J. P. Zarling, *Heat and Mass Transfer from Freely Falling Drops at low Temperatures*, CRREL Report 80-18, 1980

Attachment 2 – Paper accepted for publication at the CEM 2016

NUMERICAL STUDY OF FREEZING DROPLETS

Magalhães, Leandro[1]; Barata, Jorge[2]; Silva, André[3]
[1] University of Beira Interior, Department of Aerospace Science, Portugal, leandrobmagalhaes@gmail.com
[2] University of Beira Interior, Department of Aerospace Science, Portugal, jbarata@ubi.pt
[3] University of Beira Interior, Department of Aerospace Science, Portugal, andre@ubi.pt

KEYWORDS: *aircraft icing, heat and mass transfer, Ranz-Marshall relations*

ABSTRACT: The present work is devoted to the numerical study of freezing processes which have become of major importance in aeronautical engineering. The most common causes of structural damage to aircrafts due to climacteric changes are the result of lightning strikes and icing at the wing's leading edge or empennage. The icing of a wing's leading edge turns the smooth airflow over the wings into turbulent, decreasing lift and increasing drag. Several authors have studied heat and mass transfer on freely-falling drops, in order to determine its rate of cooling under several humidity conditions, making use of the Ranz-Marshall relations for the calculation of heat and mass transfer coefficients. The objective of the present work is to investigate numerically the freezing of free falling droplets for different diameters and air humidity ratios. The predictions are compared with experimental data and the numerical analysis is conducted to provide insight into the heat transfer involved in the freezing process under several humidity conditions.

1 INTRODUCTION

As sophisticated as technology may be, climacteric conditions remain a factor of major importance in aircraft operations. As described by Caliskan and Hajiyev (2013), lightning strikes and icing at the leading edge of a wing are the most common climacteric related causes of structural damage to aircrafts. Icing is responsible for the transformation of the smooth airflow over the wing to become turbulent, thus decreasing lift and increasing drag.

Icing on an aircraft can be studied in three different ways: flight test, the most accurate, since real life situations are considered, wind tunnel experiments, which try to recreate real life situations and numerical simulation, where the icing phenomena is considered to be a fluid structure interaction process.

Another negative effect of ice on aviation relates to the impact of hail particles, which can contribute to serious structural damage – power loss and flameouts. Hauk *et al* (2015) formulated models and validated them for the impact of ice crystals onto solid walls and were able to document the velocity where no fragmentation occurs.

Overall the formulation and integration of a suitable model for icing protection on an aircraft is composed of two parts: an adequate numerical model which fully describes the aerodynamic performance degradation to be used by a flight control model, to correct the flight dynamics according to the level of degradation.

The need for continuous investigation on aircraft's icing remains of critical importance, given the amount of incidents on record. Given the unpredictability on the conditions icing is encountered these

incidents could contribute to the increase of fatalities and material losses. A collection of ice related incident reports for large commercial airplanes between 1998 and 2007 was assembled by Dillingham (2010). The Federal Aviation Administration defines a large aircraft as any aircraft with a certificated maximum takeoff weight (MTOW) of more than 5.7 tons (12,500 pounds). The incidents were classified according to the effect icing had on the aircrafts' operation and are here presented on table 1.

Table 1. Icing and Winter Weather Related Incident Reports

Category	Number of Reports
Anti-ice or deicing incident/procedure	179
Controllability issue-ground	72
In-flight encounter-aircraft equipment problems	72
In-flight encounter-airframe and/or flight control icing	69
Other winter weather incident	42
Surface marking and signage obstruction	41
Runway, ramp, or taxiway excursion	36
Runway, ramp, or taxiway incursion	34
Controllability issue-air	32
Maintenance incident	19
Ramp safety-personnel risk or injury	17
In-flight encounter-sensor type incident	15
Total	628

The objective of the present work is to investigate numerically the freezing of free falling droplets for different diameters and air humidity ratios. The predictions are compared with experimental data and the numerical analysis is conducted to provide insight into the heat transfer involved in the freezing process under several humidity conditions.

2 MATHEMATICAL MODEL

This section describes the physical and mathematical modeling of a system of drops free falling through the air in moist conditions, according to Zarling (1980). It allows for the calculation of the maximum heat and mass transfer rates.

The first step to take into account is the approach to be used in the analysis of the heat and mass transfer rates: complete mixing model, non-mixing model or mixing model (Yao and Schrock, 1976). For the complete mixing model, it is necessary to assume the internal motion to be powerful enough for the mixing to occur, as opposite to the non-mixing model which assumes there is no internal motion and the energy equation is reduced to a transient heat conduction problem. The mixing model is neither the complete-mixing model nor the non-mixing model. This last model attempts to consider both the effects of oscillation and internal circulation on the mixing in the drop.

A water column with the shape of a cylinder is considered as a representative model, along which heat and mass transfer coefficients will be analyzed. An overall representation of the variables involved is presented in figure 1.

We begin by assuming a set of adequate initial conditions for the beginning of the calculation procedures. At this point values for the initial air and water temperatures, humidity ratio, drop diameter, air column height, flow ratio, air velocity and drop diameter are set. At the end of the column the values for the variation on the droplets' temperature are presented.

A differential control volume is established to divide the water column in smaller portions where the calculation procedure is going to be repeated until the bottom of the column is reached. This allows for a better accuracy of the results.

For instance if a greater accuracy is desired, smaller step sizes, meaning a greater number of control volumes can be used.

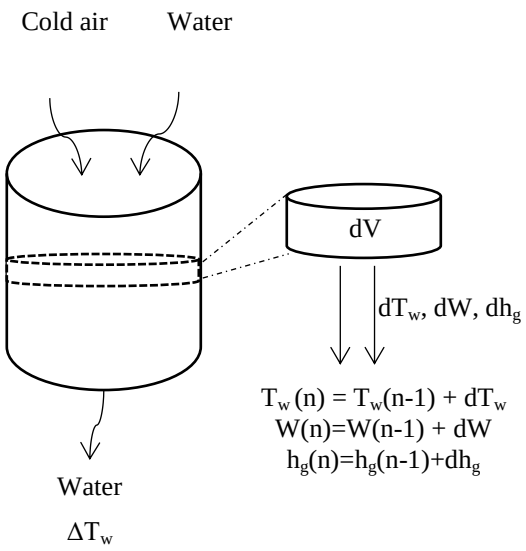

Figure 1. Schematic representation of the control volume

The heat and mass transfer coefficients for steady state conditions (equations 1 and 2) are calculated from the Ranz-Marshall relations, according to Ranz and Marshall (1952).

$$Nu = \frac{h_c d}{k} = 2 + 0.6 Re_d^{1/2} Pr_d^{1/3} \qquad (1)$$

$$Sh = \frac{h_d d}{D} = 2 + 0.6 Re_d^{1/2} Sc_d^{1/3} \qquad (2)$$

where h_c, h_d, d, k and D are the convective heat transfer coefficient, the convective mass transfer coefficient, droplet diameter, thermal conductivity and mass diffusivity, respectively.

In order to reach the desired coefficients, the Reynolds, Prandtl and Schmidt numbers are calculated according to equations 3 to 5.

$$Re = \frac{v_r . d}{\nu} \qquad (3)$$

$$Pr = \frac{\nu}{\alpha} \qquad (4)$$

$$Sc = \frac{\nu}{D} \qquad (5)$$

where v_r, is the relative velocity, ν is kinematic viscosity and α is thermal diffusivity. For the Reynolds number calculation the terminal velocity is taken into account. If we consider a jet discharged from a nozzle breaking into individual drops and looking only at velocity's vertical component, its behavior is explained as follows: the jet's velocity will decrease up to the point where it breaks into individual drops and then, subject to gravity their velocity increases until it reaches the terminal value.

The thermal diffusivity, viscous diffusivity, mass diffusivity and thermal conductivity are calculated according to Zarling (1980).

The next step is to calculate the variation in humidity across a control volume which is given by:

$$m_a dW = \rho_a h_d A_v dV (W_s - W) \qquad (6)$$

where m_a is air flow rate, ρ_a is air density and A_v is the surface area of water drops contained in the control volume and W_s the saturation humidity

As a result, the enthalpy variation of water vapor can be reached with:

$$\frac{dh}{dW} = Le \frac{(h_s - h)}{(W_S - W)} + (h_g - 2501 Le) \qquad (7)$$

where h_g, being the enthalpy of water vapor. The Lewis number and the enthalpy of the air stream are calculated as suggested by Threlked (1970):

$$Le = \frac{h_c}{\rho_a C_{p,a} h_d} \cong \left(\frac{\alpha}{D}\right)^{2/3} \qquad (8)$$

$$h = C_{p,a}T_a + 2501W \quad (9)$$

Finally, the variation in the temperature of the water is given by:

$$\Delta T_W = -\frac{m_a}{m_w c_p}(\Delta h - h_f \Delta W) \quad (10)$$

where h_f is the enthalpy of liquid water.

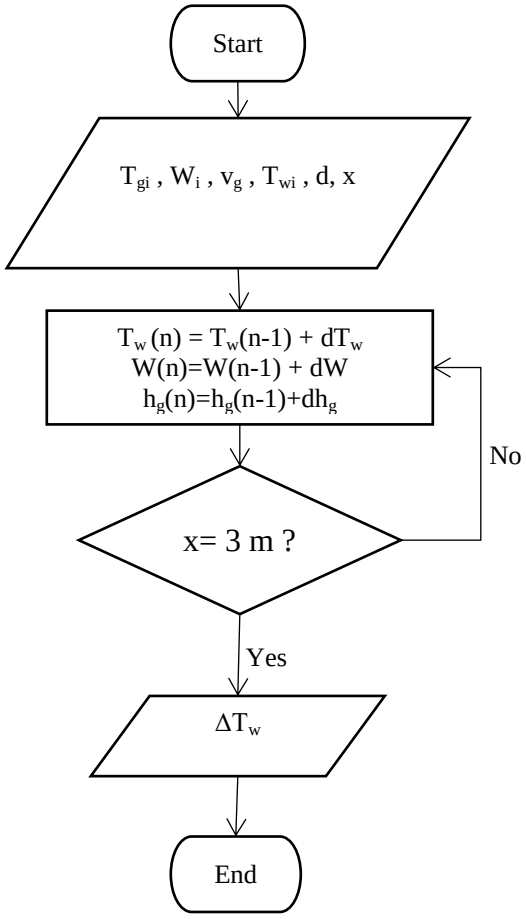

Figure 2. Flowchart of the whole process.

Then the humidity ratio, the enthalpy of the air stream and the temperature of the water are incremented for the determination of the conditions on the other side of a control volume until the bottom of the column is reached. The flowchart of the whole process is presented in figure 2.

Another important aspect to take into account when studying drops' dynamics in free fall relates to the deformation they suffer and its influence on heat and mass transfer coefficients. Since both the non-mixing and the complete mixing model represent extreme situations, a correction factor was proposed by Yao and Schrock (1976) which is an attempt to consider the effects of distortions and vibrations in the falling drops

$$g = 25\left(\frac{x}{d}\right)^{-0.7} \quad (11)$$

The correction factor developed approximates the complete mixing model with the experimental data for drops of water from *3* up to *6 mm* in diameter for a ratio of *x/d* up to *600*, *x* being the column's height. Then, it is used along with the Ranz-Marshall relations already presented in equations 1 and 2, for a more realistic calculation of the heat and mass transfer coefficients.

$$Nu = 2 + 15Re_d^{1/2}Pr_d^{1/3}\left(\frac{x}{d}\right)^{-0.7} \quad (12)$$

$$Sh = 2 + 15Re_d^{1/2}Sc_d^{1/3}\left(\frac{x}{d}\right)^{-0.7} \quad (13)$$

3. RESULTS AND DISCUSSION

The mathematical model described in the previous chapter was implemented and simulations were carried out for drops with diameters of 3, 4, 5 and 6 mm and for humidity ratios of 0.29, 0.36 and 0.52. The numerical calculations were carried out with the Ranz-Marshall relations in either their classical formulation - expressed in equations 1 and 2 - or with the addition of the correction factor – equations 12 and 13 - in an attempt to establish an analysis between the two modulations and to assert the differences

between the complete mixing model and the mixing model beforehand mentioned. The predictions were compared with the experimental results of Yao and Schrock (1976), for the model's validation.

For each simulation, both the drop's initial and air temperatures were kept constant – a characteristic of first order phase transitions, as opposite to second order phase transitions. The range of temperatures used, according to the available experimental data, experienced only slightly variations from one simulation to the next. The initial air temperature was set from a minimum of 22.14 ºC up to 23.61 ºC. As for the drop's initial temperature, it ranged from 40.66 ºC up to 40.74 ºC. The flow ratio air/water was also kept constant at 0.1 Kg and the velocity of the air stream was set to 3 cm/s. The total falling distance as expressed on the corrected Ranz-Marshall relations is here defined as 3 m. The number of control volumes was set to 30, so it happens each volume corresponds to 0.1 mm.

Figure 3 represents the variation on drops' temperature falling through the air for a diameter of 3 mm and humidity ratio of 0.36. The falling distance on the horizontal axis is divided by the drop's diameter, while the temperature variation within them is divided by their own initial temperature, which results in both axes being represented as dimensionless quantities. The drops' temperature variation corresponds to the oscillation on the entire column as defined on section 2. Filled circles correspond to the experimental data, while hollow circles represent predictions, being the dashed line relative to the classical Ranz-Marshall relations while the solid one relates to the Ranz-Marshall equations adding the correction factor. For a diameter of 3 mm and humidity ratio of 0.36 the complete mixing model over predicts cooling for falling distances greater than 50 diameters, while the mixing model under predicts cooling for falling distances lower than 350 diameters. The predictions suggest early steady state conditions, while for x/d > 350 the effects of distortions and vibrations become predominant.

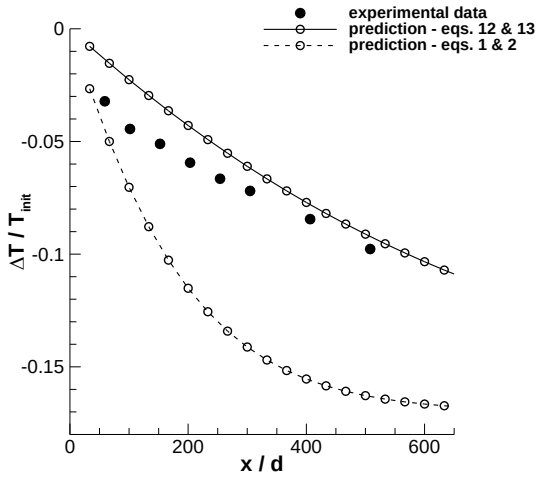

Figure 3. Variation on drops' temperature falling through the air for a diameter of 3 mm and humidity ratio of 0.36

Figure 4 shows the temperature variation for drops falling through the air for a humidity ratio of 0.36 and a diameter of 3, 4, 5 and 6 mm. The circle, square, triangle and diamond symbols correspond to diameters of 3, 4, 5 and 6 mm, respectively. As in the previous figure, the filled symbols correspond to the experimental data, while the hollow ones to the predictions, where the dashed line is relative to the simulations considering the classical Ranz-Marshall relations while the solid lines relate to the Ranz-Marshall equations adding the correction factor. The results show the complete mixing model predictions are in agreement for falling distances lower than 50 diameters. For this region cooling may be considered steady state and independent of diameter Otherwise, the results suggest the effects of distortions and vibrations in the falling drops are heavily dependent on drop size. Effects of distortions

and vibrations in the falling drops become predominant early as diameter values increase, e.g. for a diameter of 6 mm the effects of distortions and vibrations in the falling drops become predominant x/d > 100. Now, the key question that remains is: what effect different humidity values have on the results?

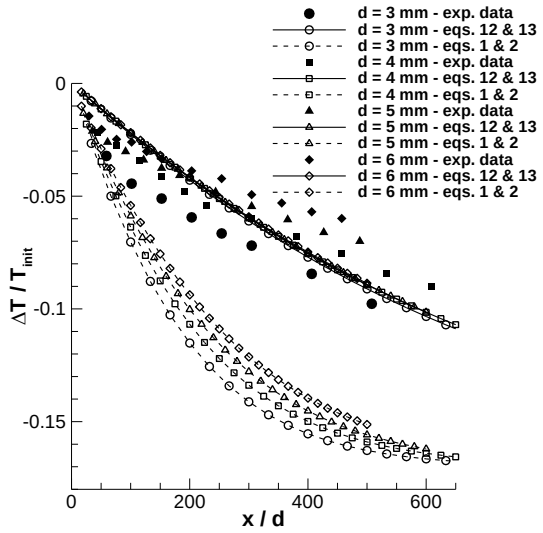

Figure 4. Variation on drops' temperature falling through the air for diameters of 3 to 6 mm and constant humidity ratio of 0.36

Figure 5 shows the drops' temperature variations for a humidity ratio of 0.29 and diameters of 3 and 5 mm. Through this figure analysis, it is seen the experimental data is better approximated by the complete mixing model given by equations 1 and 2, especially for values of less than 100 diameters, in the case of 3 mm drops, while for the case of 5 mm drops, overall the complete mixing model is a good approximation.

Figure 6 shows the drops' temperature variations for a humidity ratio of 0.52 and diameters of 4 and 6 mm. In this figure, the mixing model proves to be effective only for values of less than 80 diameters, hinting cooling in this conjugation of values may be a problem on a transient regime and the non-mixing model may be needed for a better approach.

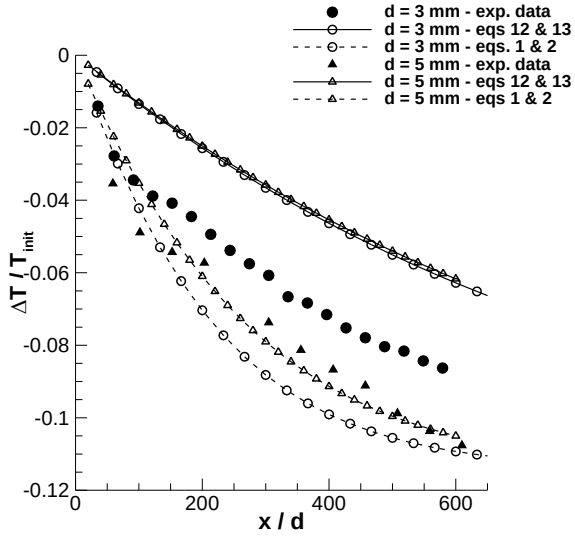

Figure 5. Variation on drops' temperature falling through the air for diameters of 3 to 6 mm and constant humidity ratio of 0.29

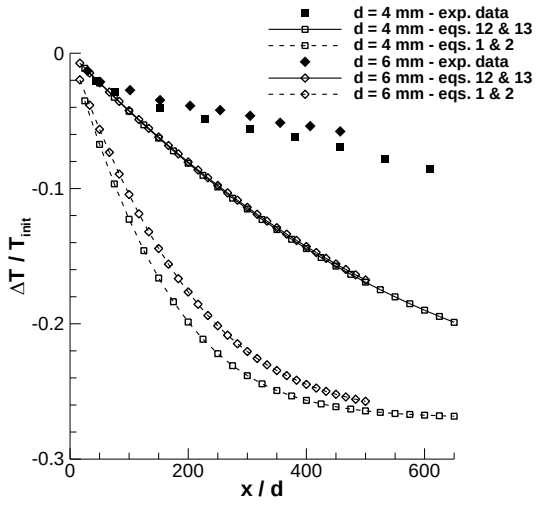

Figure 6. Variation on drops' temperature falling through the air for diameters of 4 and 6 mm and constant humidity ratio of 0.52

4. CONCLUSIONS

A model for the cooling of a system of falling water drops was presented, where the influences of variations in humidity ratio and diameter of drops was studied.

For the lower humidity tested (0.29), the numerical data obtained from using the complete mixing model proves to be the better approximation, suggesting a regime of steady state conditions.

On the other hand looking to the highest humidity value (0.52), the mixing model is only able to approximate data up to 50 diameters, after which the drops will cool less than predicted. In this case the obtained data hints the presence of a transient regime, where the non-mixing model could be of use.

For last, the middle humidity parameter tested (0.36) is the one where a closer agreement between the mixing model and experimental data is obtained. On the other hand drop's vibrations and oscillations may also have a bigger role in the overall process dynamics than initially considered.

In a final remark further experimental data is needed for the models' validation for freezing, since it was only possible to recreate cooling conditions, given the available experimental data.

5. ACKNOWLEGMENTS

The present work was performed under the scope of the LAETA – Laboratório Associado em Energia, Transportes e Aeronáutica – activities.

6. REFERENCES

Caliskan, F. and Hajiyev, C., *A review of in-flight detection and identification of aircraft icing and reconfigurable control*, Istanbul Technical University, Progress in Aerospace Sciences 60 (2013), 12-34

Hauk, T., Bonaccurso, E., Roisman, I.V. and Tropea, C., *Ice crystal impact onto a dry solid wall. Particle fragmentation*, Proceddings of the Royal Society A, 2015

Dillingham, L., *Aviation safety, preliminary information on aircraft icing and winter operations, GAO, United States Government Accountability Office testimony before the subcommittee on aviation*, Committee on Transportation and Infrastructure, 2010

Zarling, J. P., *Heat and Mass Transfer from Freely Falling Drops at low Temperatures*, CRREL Report 80-18, 1980

Yao, S. C. and V. E. Schrock, *Heat and mass transfer from freely falling drops*, Journal of heat transfer, ASME, vol. 98, no 1, 120-125, 1976

Ranz, W. E. and Marshall, W. R., *Evaporation from drops*, Chemical Engineering Progress, vol.48, no 3 &4, 141-146, 173-180, 1952

Threlkeld, J. L., *Thermal environmental engineering* Englewood Cliffs, N.J.: Prentice-Hall, Inc 1970